Received: 10 July 2023 | Revised: 1 February 2024 | Accepted: 5 February 2024

DOI: 10.1111/joa.14026

Journal of Anatomy | ANATOMICAL SOCIETY WILEY

ORIGINAL ARTICLE

Trabecular architecture of the distal femur in extant hominids

Andrea Lukova[1] | Christopher J. Dunmore[1] | Sebastian Bachmann[2] | Alexander Synek[2] | Dieter H. Pahr[2,3] | Tracy L. Kivell[4] | Matthew M. Skinner[4]

[1]Skeletal Biology Research Centre, School of Anthropology and Conservation, University of Kent, Canterbury, UK

[2]Institute of Lightweight Design and Structural Biomechanics, TU Wien, Wien, Austria

[3]Department of Anatomy and Biomechanics, Division Biomechanics, Karl Landsteiner University of Health Sciences, Krems, Austria

[4]Department of Human Origins, Max Planck Institute for Evolutionary Anthropology, Leipzig, Germany

Correspondence
Andrea Lukova1, Skeletal Biology Research Centre, School of Anthropology and Conservation, University of Kent, Canterbury, UK.
Email: al646@kent.ac.uk

Funding information
European Union's Horizon 2020 research and innovation programme, Grant/Award Number: 819960

Abstract

Extant great apes are characterized by a wide range of locomotor, postural and manipulative behaviours that each require the limbs to be used in different ways. In addition to external bone morphology, comparative investigation of trabecular bone, which (re-)models to reflect loads incurred during life, can provide novel insights into bone functional adaptation. Here, we use canonical holistic morphometric analysis (cHMA) to analyse the trabecular morphology in the distal femoral epiphysis of *Homo sapiens* ($n = 26$), *Gorilla gorilla* ($n = 14$), *Pan troglodytes* ($n = 15$) and *Pongo* sp. ($n = 9$). We test two predictions: (1) that differing locomotor behaviours will be reflected in differing trabecular architecture of the distal femur across *Homo*, *Pan*, *Gorilla* and *Pongo*; (2) that trabecular architecture will significantly differ between male and female *Gorilla* due to their different levels of arboreality but not between male and female *Pan* or *Homo* based on previous studies of locomotor behaviours. Results indicate that trabecular architecture differs among extant great apes based on their locomotor repertoires. The relative bone volume and degree of anisotropy patterns found reflect habitual use of extended knee postures during bipedalism in *Homo*, and habitual use of flexed knee posture during terrestrial and arboreal locomotion in *Pan* and *Gorilla*. Trabecular architecture in *Pongo* is consistent with a highly mobile knee joint that may vary in posture from extension to full flexion. Within *Gorilla*, trabecular architecture suggests a different loading of knee in extension/flexion between females and males, but no sex differences were found in *Pan* or *Homo*, supporting our predictions. Inter- and intra-specific variation in trabecular architecture of distal femur provides a comparative context to interpret knee postures and, in turn, locomotor behaviours in fossil hominins.

KEYWORDS
bipedalism, functional morphology, *Gorilla*, human, knee, locomotor behaviour, *Pan*, *Pongo*

1 | INTRODUCTION

Understanding how variation in skeletal morphology, both external shape and internal bone structure, may reflect differences in loading during habitual behaviours in extant apes is critical to reconstructing behaviour in fossil hominoid taxa. Extant apes are characterized by a wide range of locomotor, postural and manipulative behaviours linked to their respective ecological niches,

subsistence strategies and social organization, which require each species to use their limbs in different ways. Although African apes also engage in arboreal suspension and climbing, they spend the majority of their time terrestrially knuckle-walking, in which the knee is flexed to varying degrees (Ankel-Simons, 2010; Georgiou et al., 2018; Isler, 2005; Lee et al., 2012). Orangutans engage in slow-moving, torso-orthograde locomotion, often supported by multiple limbs (Cant, 1987; Thorpe & Crompton, 2005), in which load is distributed across both upper and lower limb joints. Humans are the only living obligate bipedal ape and are unique among primates in that both the hips and knees remain relatively extended during the gait cycle. In this study we build on previous research (Georgiou et al., 2018; Sukhdeo et al., 2020; Sylvester & Terhune, 2017) to examine the link between habitual joint postures of the knee and trabecular architecture in the distal femur of extant great apes, including humans.

Although the structure of trabecular bone is also influenced by several factors, including genetics, hormones, diet, sex, age, body size and physical activity (Loewen et al., 2001; Paternoster et al., 2013; Turner et al., 2000), (re-)modelling is at its peak during ontogeny and persists (although at a reduced rate) throughout adulthood (Barak, 2019; Glatt et al., 2007; Halloran et al., 2002; Saers et al., 2020; Seeman, 2003; Wallace et al., 2013). It has been previously demonstrated that joint load is transferred from the subchondral bone of the epiphyses towards the diaphyseal cortical bone (Barak et al., 2008). Correlations between cortical bone features and different types of locomotion among great apes have been previously found. For example, Carlson (2005) found that African apes engaging more frequently in arboreal locomotion have more circular femoral cross-sections compared with those that engage more in terrestrial locomotion. Ruff (2002) also found a relationship between locomotor activities in great apes and cross-sectional properties of forelimb and hindlimb bones. Asian apes show relatively stronger forelimb shafts than hindlimb shafts compared to African apes and within African apes, more arboreal *Pan* shows relatively higher ratios of forelimb to hindlimb strength compared to more terrestrial *Gorilla* (Ruff, 2002). Moreover, cross-sectional differences between humans and non-human apes reflecting differences in locomotor loading have been found in the femoral neck (Lovejoy, 1988; Ohman et al., 1997; Rafferty, 1998) and in the distal tibia and talus (Tsegai et al., 2017).

Trabecular bone models in response to loading through either an increase or decrease of bone tissue and/or reconfiguration of the shape and structure of trabecular struts in order to reduce strain and prevent fracture (Barak et al., 2011; Biewener et al., 1996; Harrison et al., 2011; Mittra et al., 2005; Pontzer et al., 2006; Rodan, 1997; Ruff et al., 2006; Sinclair et al., 2013). Thus, it is expected that trabecular bone structure within the epiphysis of the distal femur will reflect variation in loaded knee joint postures among extant great apes. The ratio of bone volume to total volume (BV/TV) is the proportion of trabecular bone of the total volume in a given region. In places where stress is lower, there is a gradual decline in the amount of trabecular bone, resulting in a weaker structure; conversely, in places where stress is higher, there is a gradual increase in trabecular bone deposition to help resist loads (Barak et al., 2011; Pontzer et al., 2006; Sinclair et al., 2013). Degree of anisotropy (DA) describes the trabecular alignment in 3D space, with high DA indicating greater alignment (trabeculae tend to be oriented in specific direction) or an anisotropic structure, and low DA (values closer to 0) reflecting less alignment (trabeculae tend to be more randomly oriented) and an isotropic structure. BV/TV and DA can together explain up to 97% of the variation in elastic properties of trabecular bone (Homminga et al., 2003; Maquer et al., 2015; Van Rietbergen et al., 1998; Zysset, 2003). BV/TV and DA have been shown to reflect the presumed predominant direction and relative magnitude that joints are loaded in, during different locomotor and manipulative behaviours; in previous landmark studies (Dunmore et al., 2019, 2020; Sylvester & Terhune, 2017), throughout an entire bone or epiphysis (Kuo et al., 2022; Ryan et al., 2019; Saers et al., 2022; Skinner et al., 2013; Stephens et al., 2016; Tsegai et al., 2018) or by using holistic morphometric approaches (Bachmann et al., 2022; DeMars et al., 2022; Dunmore et al, 2023). Recent methodological advancements allow comprehensive statistical analysis of trabecular bone structure within and between species, particularly those that vary in external bone shape (Bachmann et al., 2022; Gross et al., 2014). Here we investigate the trabecular structure in the entire distal femoral epiphysis of extant humans and other great apes to explore how potential variation might reflect significant differences in knee joint loading during locomotor behaviours.

Several previous studies have examined trabecular structure in the lower limbs of primates, including the pelvis/innominate (Dalstra et al., 1993; Eriksen et al., 1984; Volpato et al., 2008; Zaharie & Phillips, 2018), proximal femur (Cazenave et al., 2019; Coelho et al., 2009; Demes et al., 2000; Georgiou et al., 2019; Georgiou et al., 2020; Ruff et al., 2013; Ryan & Ketcham, 2002; Ryan & Walker, 2010; Volpato et al., 2008), proximal tibia (Kamibayashi et al., 1995; Mazurier et al., 2010; Novitskaya et al., 2014; Saers et al., 2016; Sugiyama et al., 2012; Thomsen et al., 2005) as well as the ankle and foot (DeSilva, 2009; DeSilva & Devlin, 2012; Su et al., 2013; Tsegai et al., 2017). However, only two previous studies have specifically examined trabecular bone structure in the hominoid knee joint. Sylvester and Terhune (2017) describe a new geometric morphometric approach to analyse subchondral trabeculae of human distal femur. They found sex differences in subchondral trabecular spacing in the human knee, with males having more evenly spaced trabeculae compared to females. This study provided important insight into bone loading that might be overlooked with a centrally placed volume-of-interest methods, particularly in joints where trabecular structure is not homogenously distributed across epiphyses (Sylvester & Terhune, 2017). Georgiou et al. (2018) analysed trabecular structure of distal femoral epiphysis of extant great apes and found that humans have higher BV/TV and DA on the posteroinferior margin of the condyles compared to non-human apes. Additionally, they showed that *Pan* and *Pongo* have higher BV/TV

values in the posterior region of the condyles compared to other hominoids. This study revealed some functional signals in distal femur linked to locomotor behaviour of great apes, but they also found a large degree of overlap across some taxa. Their statistical comparisons between taxa were limited to a priori defined quadrants of each condyle, so trabecular patterns within each quadrant could only be analysed qualitatively (Georgiou et al., 2018).

We build upon these previous studies with an expanded sample and the canonical holistic morphometric analysis (cHMA) method to statistically analyse trabecular patterns of the distal femur in extant apes, free of a priori sub-sampling. cHMA addresses the potential bias caused by inter-specific differences in shape by computing canonical models representing the mean size, position and morphology from a multispecies sample of individual bones. Moreover, cHMA treats each mesh cell as homologous when computing a canonical model and so geometric homology is achieved. Without geometric homology, quadrants are an arbitrary unit of analysis and the functional signal might be lost when trabecular concentration is divided. cHMA allows us to test whether the distribution of bone parameters differ statistically between (as well as within) different species. By using cHMA, we are able to build taxon-specific mean models (with standard deviations) and conduct multivariate comparisons with high statistical power as all homologous finite elements of each studied trabecular parameter could be compared across every individual in the sample (see more details next) (Bachmann et al., 2022).

2 | EXTERNAL KNEE MORPHOLOGY AND PREDICTED KNEE POSTURES DURING LOCOMOTION

Extant hominids exhibit anatomical variation of the knee joint, particularly regarding the relative size and shape of the femoral condyles, the size and shape of the patella as well as the articulation of the femoral condyles and the tibial plateau at various angles of knee flexion. The knee joint experiences load not only from substrate reaction forces, but also from the action of muscles, tendons and ligaments during various locomotor activities. Additionally, soft tissue morphology of the knee joint in extant non-human great apes (hereafter, just 'great apes') differs in the degree to which it provides stability and mobility at different joint angles (Barak et al., 2011; Currey, 2003, 2012; Demes, 2007; Pearson & Lieberman, 2004; Rubin et al., 2002; Ruff et al., 2006; Shaw & Ryan, 2012). In comparison, the human knee joint has several bony and soft tissue features that stabilize the knee especially in a fully extended posture (DeSilva et al., 2018; Haile-Selassie et al., 2012; Harcourt-Smith et al., 2015; Harcourt-Smith, 2016; Lovejoy et al., 2009; Sylvester & Organ, 2010; Sylvester, 2013; Sylvester et al., 2011). These differences in hard and soft tissue morphology, discussed in more detail next, will influence load distribution across the femoral condyles and the tibial plateau, which in turn should influence trabecular (re-)modelling across hominids.

2.1 | Shape of the distal femur, proximal tibia and associated soft tissue structures

In humans both condyles of the distal femur are approximately the same size, but in other great apes the medial condyle is larger than the lateral condyle (Sylvester, 2013; Sylvester & Pfisterer, 2012; Tardieu, 1999). The distal articular surface is square in humans (i.e. with relatively equal anteroposterior and mediolateral dimensions) and is more symmetrical around the parasagittal plane passing through the middle of trochlea than it is the great ape femur (Figure 1g). Both condyles are elliptical when viewed laterally in humans, which projects the patella anteriorly, thereby increasing the lever arm of quadriceps femoris, compared to great apes. Also, the lateral femoral condyle is flat in its sagittal plane (Figure 1g), which increases the contact area between the lateral femoral condyle and lateral tibial plateau when the knee is extended (Lovejoy, 2007; Tardieu, 1999). The more convex lateral condyle in great apes (Figure 1g) produces similar joint stress across all the joint positions and helps to reduce joint stress in the patellofemoral contact area during flexion (Lovejoy, 2007). In humans, the patellar groove of the femur is relatively deep and the lateral lip of trochlea projects more anteriorly than the medial lip (Wanner, 1977). Stern Jr and Susman (1983) suggested that the main function of the deep patellar groove and prominent lateral lip is to prevent patellar dislocation on the flexed knee due to the line of action of the quadriceps whose origin is laterally placed due to the higher valgus angle in humans compared to higher varus angle in non-human great apes.

In humans, the quadriceps femoris inserts on the proximal patellar surface, continues over the anterior surface and inserts via the patellar ligament on the tibial tuberosity. Vastus medialis and lateralis insert on the medial and lateral margins of the patella, respectively, which helps to protect the knee from medial/lateral dislocation as quadriceps femoris extends the knee. When the knee is at its full extension, the patello-femoral joint contact occurs at the distal end of patella (Figure S1). As flexion increases, the patello-femoral contact area increases as well. During flexion, the patella engages into the femoral trochlear groove and the contact area spreads across the width of the patella and moves proximally (Lovejoy, 2007; Tardieu, 1999) (Figure S1). Thus, with the higher articular area, the stress during knee flexion is reduced (Masouros et al., 2010). In great apes, the patella is both absolutely and relatively smaller than in humans due to the smaller quadriceps muscle. In all primates, the quadriceps muscles compress the patella against the femur during flexion, with subsequent joint stress depending on the size of the patello-femoral contact area (Lovejoy, 2007). The knee of great apes is more or less flexed during all locomotor activities compared to humans. A flatter trochlea then allows the patello-femoral surface to bear higher forces when the quadriceps press the patella against the femur (Lovejoy, 2007).

In humans, the menisci form a mobile unit on the tibial plateau that adapts to the sliding and rotating movements of the femoral condyles and function as an important secondary co-resistant to

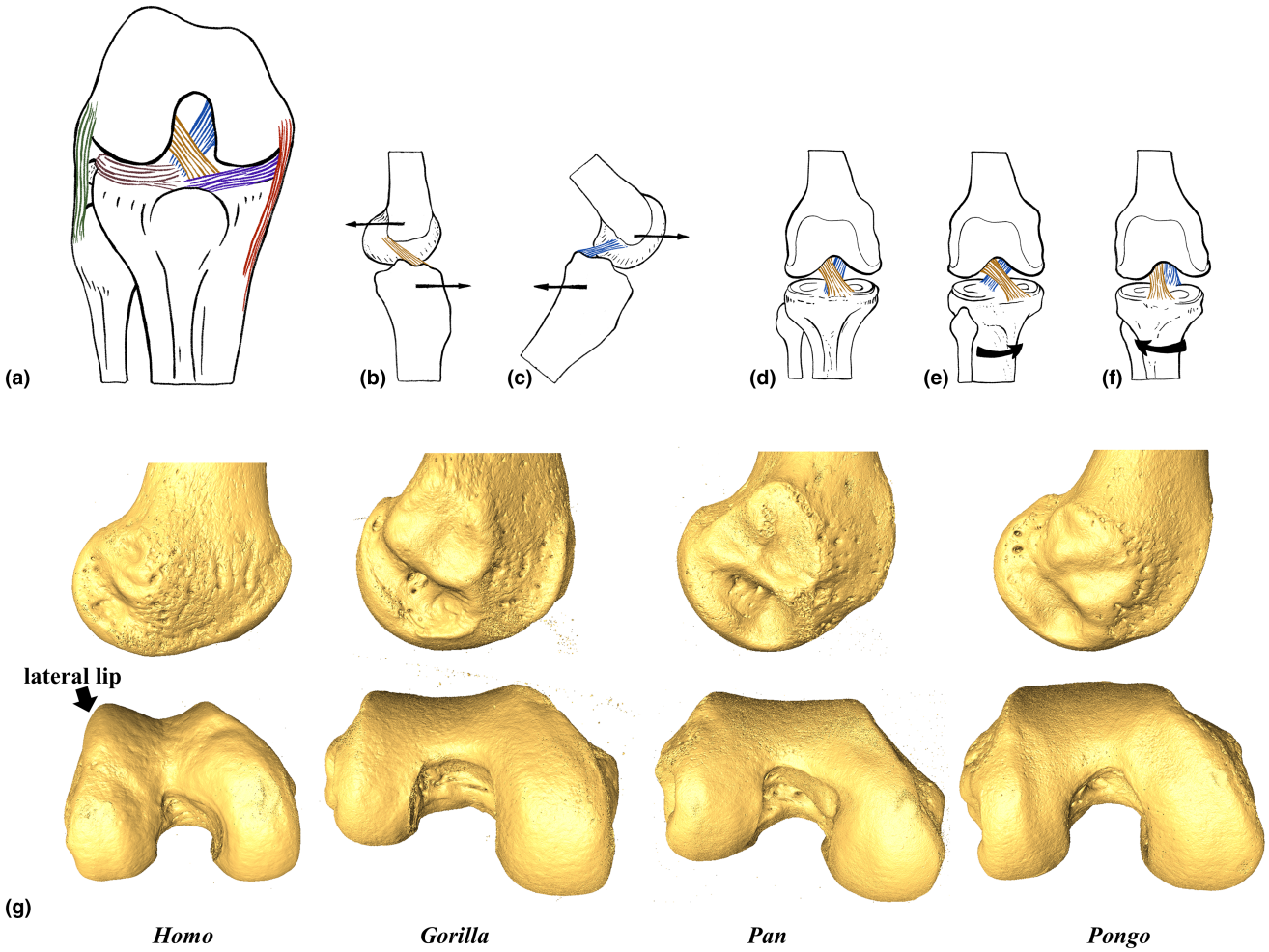

FIGURE 1 (a) Ligament attachments of the knee showing inferior view. Gold, anterior cruciate ligament; blue, posterior cruciate ligament; green, lateral collateral ligament; red, medial collateral ligament; brown, lateral meniscus; purple, medial meniscus. The medial collateral ligament inserts at the medial epicondyle of the femur and attaches along the medial border of the tibial plateau and on the medial surface of the tibial shaft. The lateral collateral ligament inserts on the lateral femoral epicondyle and attaches on the head of fibula. (b) Anterior cruciate ligament position during forward tibia and backward femur movements. (c) Posterior cruciate ligament position during backward tibia and forward femur movements. Cruciate ligaments position during (d) neutral knee position; (e) medial knee rotation; (f) lateral knee rotation. The anterior cruciate ligament arises from the anterior intercondylar space on the tibial plateau, runs upwards and posteriorly and attaches on the inside of the lateral condyle of the femur. The posterior cruciate ligament arises from well back on the posterior intercondylar space, runs upwards and anteriorly and attaches on the inside of the medial condyle. (g) Surface models of right distal femur of *Homo*, *Gorilla*, *Pan* and *Pongo*. Showing more elliptical shape of lateral condyle, square outline of distal surface and high lateral lip in humans compared to great apes.

the cruciate ligaments. When the knee is flexed, the popliteus tendon pulls the menisci posteriorly and the contact point of femoral condyle and tibial plateau also moves posteriorly (Lovejoy, 2007; Tardieu, 1999). Conversely, when the human knee is extended, the menisci again follow the femoral condyle and tibial plateau moving both anteriorly (e.g. Hirschmann & Müller, 2015). In great apes, the lateral meniscus has only a single point of attachment to the tibia. Additionally, the lateral meniscus is connected on its posterior surface to the Wrisberg ligament, which in turn attaches on the inside of the medial femoral condyle (this ligament is rarely found in humans) (Girgis et al., 1975). The anterior transverse ligament is absent, and the medial meniscus is not attached to the medial collateral ligament, but it is separated from it by a bursa. These differences allow greater range of knee movements in great apes compared to humans (Girgis et al., 1975).

Due to the difference in weight transfer through the lower limb and size of femoral condyles, the relative size of the tibial condyles in great apes is opposite to that in humans. The medial tibial condyle is much larger and more convex than the lateral and the tibial plateau is supero-inferiorly compressed (Berger & Tobias, 1996) with a thin lateral epicondyle (Frelat et al., 2017). The posterior cruciate ligament attaches to the medial femoral condyle more anteriorly and nearer to the midline of the intercondylar notch in great apes than in humans. The collateral ligaments control the side-to-side motions and the cruciate ligaments control both the slide of the femur and the medial rotation of the tibia as they do in humans (Figure 1a–f).

However, because of the different attachment of the posterior cruciate ligament, medial rotation of the tibia is greater in great apes compared to humans.

2.2 | Locomotor behaviour and biomechanics of knee posture during the gait cycle

Humans and great apes are characterized by a wide range of locomotor behaviours that vary in their frequency and knee postures, both across and within species. These differences influence knee load distribution and thus should affect trabecular (re-)modelling. Next, we discuss what is known about the biomechanical differences in knee joint posture and loading across our study species, which form the basis of our predictions about variation in trabecular structure.

2.2.1 | Humans

Humans not only are primarily bipedal walkers but also often engage in other activities such as running, jumping or squatting, in which the knee position may vary substantially (Mann & Hagy, 1980; Nilsson & Thorstensson, 1987; Racic et al., 2009). Human bipedal gait is at or close to full extension of the knee for most of its cycle (Javois et al., 2009; Landis & Karnick, 2006; Organ & Ward, 2006; Sylvester & Pfisterer, 2012; Tardieu, 1999) (Figure S1) and the variability in location of the resulting joint forces on the distal femur is limited (Preuschof & Tardieu, 1996). Both the medial and lateral condyles are evenly loaded through the tibial plateau during locomotion (Lovejoy, 2007; Sylvester, 2013; Sylvester & Pfisterer, 2012; Tardieu, 1999). When the knee is flexed, the range of motion is approximately 45° of lateral and 25° of medial rotation (Lovejoy, 2007). The amount of axial rotation (i.e. twisting of the knee relative to the tibia) depends on the amount of load, with high loads leading to low rotator flexibility and vice versa (Lovejoy, 2007). During extension, the patellar tendon moves to the centre of rotation and the lever advantage of the quadriceps muscle increases in intensity (Loudon, 2016). Medial and lateral collateral ligaments tighten the knee joint in full extension and limit rotation and hyperextension. In flexion, they are loose and allow more rotational knee movements. The medial collateral ligament is also tightened in lateral rotation and loose in medial rotation. The lateral collateral ligament is, by contraction of the quadriceps tendon, actively tightened during flexion–extension (Hirschmann & Müller, 2015). The posterior cruciate ligament is in tension when the knee is flexed and prevents the femur from sliding anteriorly off the tibial plateau (Figure 1c), whereas the anterior cruciate ligament is in tension when the knee is extended and prevents femur from sliding posteriorly off the tibial plateau (Figure 1b). Additionally, the cruciate ligaments limit medial rotation to the tibia in relation to the femur (Figure 1d,e). If tibia is rotated laterally, the cruciate ligaments untwist and have no limiting ability (Figure 1f).

2.2.2 | Pan

Great apes practice a variety of locomotor behaviours depending on their habitat, body size, sex and age (although we focus only on adults in this study). In this study, *Pan* is represented only by *Pan troglodytes verus* from the Taï National Forest, Ivory Coast. Doran (1993) found that Taï adult *Pan* spend approximately 15%–18% of their daily time in locomotion and, within this locomotor time, they engage on average in 16% arboreal and in 84% terrestrial locomotion. Both lower limbs are often exposed to external forces (substrate reaction forces) where the knee is flexed and the hip is abducted to varying degrees during both terrestrial and arboreal locomotion (Ankel-Simons, 2010; D'Août et al., 2004; Georgiou et al., 2018; Isler, 2005; Lee et al., 2012; Pontzer et al., 2009) (Figure S1). During climbing, *Pan* may utilize their full flexion–extension range at the knee (D'Août et al., 2002; Isler, 2005). The single meniscal attachment of the lateral meniscus facilitates medial and lateral rotation of the knee (Javois et al., 2009; Landis & Karnick, 2006; Tardieu, 1999). Characteristic flattening of the femoral trochlea allows free patellar movements during knee rotation associated with foot grasping during arboreal behaviour (Tardieu, 1999). During terrestrial knuckle-walking in zoo-housed chimpanzees, knee flexion ranges from ~161.4° at foot touchdown to ~117.4° at toe-off, and there is inter-individual variation in vertical ground reaction force (Finestone et al., 2018; Kozma et al., 2018). Even though there is an evident lateral rotation movement during extension in *Pan*, the knee is still mostly loaded in flexed and varus postures during terrestrial locomotion (Lovejoy, 2007). The differing size between femoral condyles causes mediolateral knee rotation during all phases of terrestrial quadrupedal locomotion. Additionally, the medial condyle is loaded more than the lateral condyle (Sylvester, 2013; Sylvester & Pfisterer, 2012; Tardieu, 1999). There are no significant sex differences in the overall frequency of arboreal and terrestrial locomotion (Doran, 1993). However, there are significant sex differences in the type of arboreal locomotor behaviours used, with adult male *Pan* using significantly less quadrupedalism (males 23.4%, females 60.6%) and more vertical climbing (males 60.2%, females 52.4%) than females (Doran, 1993).

2.2.3 | Gorilla

Gorilla also engages most frequently in terrestrial knuckle-walking and the frequency of arboreality depends mostly on their habitat and body size (Doran, 1996; Doran, 1997; Isler, 2005; Remis, 1994; Tocheri et al., 2011). In this study, *Gorilla* is represented only by *Gorilla gorilla gorilla*, for which locomotor behaviour in wild has only been studied in one group (Bia Hokou, Central African Republic; Remis, 1994). During terrestrial knuckle-walking, the knee is flexed, as in *Pan*, and the hip is in abduction to varying degrees (Figure S1) (Finestone et al., 2018). Compared to *Pan*, zoo-housed *Gorilla* are found to extend their limbs more during terrestrial locomotion and vertical climbing (Crompton et al., 2008; Finestone et al., 2018; Isler, 2005; Kozma et al., 2018). The knee

angles vary from ~163.2° at foot touchdown to ~126.6° at toe-off (Kozma et al., 2018). Hip abduction is a clear advantage in climbing, and in *Gorilla*, it is necessary to accommodate their large belly, which limits hip flexion in its sagittal plane during climbing as well as in quadrupedal postures (Preuschof & Tardieu, 1996). However, flexion–extension range at the hip has been shown to differ more than 30° between sexes, with higher range of motion in females (Hammond, 2014), which could additionally rotate the knee more medially. Isler (2005) reported that maximal extension of the hip and knee during vertical climbing is significantly higher in the captive adult female *Gorilla* (approximately 135° knee extension) compared to males (approximately 100° knee extension). Additionally, Isler (2005) found that males exhibit a smaller range of motion at the knee during vertical climbing (approximately 55° knee range of motion) compared to females (approximately 65–85° knee range of motion).

2.2.4 | Pongo

Pongo is the most arboreal of all the great apes. They are characterized by greater joint mobility than other hominids due to their diverse locomotor behaviour where all limbs are used variously to achieve balance (Payne et al., 2006; Thorpe et al., 2009; Thorpe & Crompton, 2006). In this study, *Pongo* is represented by *Pongo pygmaeus* and *Pongo abelii*. During terrestrial locomotion, the *Pongo* knee posture in zoo-housed individuals does not differ significantly to that of African apes (Kozma et al., 2018). During terrestrial locomotion, *Pongo* is found to have a similar degree of knee extension to that of female *Gorilla*, but with a larger range of hip joint motion (Isler, 2005; Morbeck & Zihlman, 1989). However, during arboreal locomotion, their knee postures range from hyper-flexed to extended postures (Isler, 2005; Morbeck & Zihlman, 1989; Payne et al., 2006; Thorpe & Crompton, 2005, 2006; Thorpe et al., 2009) and thus the range of knee motion is significantly larger compared to *Pan* and *Gorilla* (Figure S1). Previous studies have found female Bornean *Pongo* to be more arboreal compared to their male counterparts (Cant, 1987; Galdikas, 1988). However, no sex differences in the frequency of arboreality have been found in Sumatran *Pongo* (e.g. Thorpe & Crompton, 2005; Thorpe & Crompton, 2006). Unfortunately, we are not able to test sex differences within *Pongo* in this study as we have only two males in our sample.

3 | HYPOTHESES AND PREDICTIONS

In this study we test two hypotheses. The first hypothesis is that trabecular architecture of the distal femur will reflect differences in knee postures and presumed loading during locomotor behaviours across *Homo*, *Pan/Gorilla* and *Pongo*. We predict that:

(1A) *Homo* will exhibit the highest BV/TV posteroinferiorly in the condyles due to their habitual extended knee posture. BV/TV on the patellar surface of femur will be higher laterally due to the higher loading of lateral knee compartment. BV/TV will be greater in the lateral condyle compared to medial condyle, reflecting the resistance of the knee adduction moment provided by the quadriceps and gastrocnemius muscles. *Homo* will exhibit the highest DA in anterior and posteroinferior/superior regions of both condyles (consistent with low variability in loading direction) resulting from the stereotypical loading of these regions during extended knee postures during all phases of bipedal locomotion.

(1B) *Pan* and *Gorilla* will exhibit the highest BV/TV posterosuperiorly on the condyles within their knee due to their more flexed knee position compared to *Homo*. BV/TV will be higher medially on patellar surface of femur due to the higher loading of medial knee compartment. *Pan* and *Gorilla* will display the highest DA in the posteroinferior/superior regions of the condyles (consistent with low variability in loading direction) due to their higher loading of the posterior regions during stereotypically flexed knee postures during arboreal and terrestrial locomotor behaviours.

(1C) *Pongo* will exhibit a more homogenous distribution of BV/TV across the condyles and patellar surface of femur relative to other great apes due to their more variable knee joint postures during locomotion (which may vary from full extension to full flexion). *Pongo* will exhibit the highest DA in the posterior regions of condyles (consistent with low variability in loading direction) in a similar pattern as *Pan* and *Gorilla* due to their higher loading of the posterior regions in mostly flexed knee postures particularly during terrestrial locomotion. However, due to more varied postures/loading in *Pongo*, we predict that DA will be the lowest (consistent with high variability in loading direction) and the most homogenous across the distal femora of all studied taxa.

The second hypothesis is that trabecular architecture will reflect sex differences (or lack thereof) in the locomotor behaviours and, in particular, the frequency of arboreality between female and males in our study taxa. Note, we cannot test for sex differences in *Pongo* due to sample size restrictions. We predict that:

(2A) If trabecular morphology reflects variation in frequency of terrestrial versus arboreal locomotion, we expect female *Gorilla* to show more flexed knee-posture loading than males due to greater frequency of climbing. If trabecular morphology reflects variation in the level of knee flexion/extension, we expect female *Gorilla* to have higher BV/TV in the lateral condyle, as well as in the lateral part of patellar surface and in the lateral epicondyle, compared to males due to their greater degrees of knee extension (particularly when climbing) and male *Gorilla* to have relatively higher BV/TV in the medial condyle and epicondyle because of their higher degree of flexion and thus higher loading of medial knee compartment (particularly when climbing).

(2B) If trabecular morphology reflects variation in frequency of terrestrial versus arboreal locomotion, we expect to find no significant differences in BV/TV and DA between female and male *Pan*, since no significant sex differences in the overall frequency of arboreal and terrestrial locomotion has been found in the Taï chimpanzees (Doran, 1993). Furthermore, even though sex differences in the types of arboreal locomotion have been reported in *Pan*, with

adult male *Pan* using significantly less quadrupedalism (males 23.4%, females 60.6%) and more vertical climbing (males 60.2%, females 52.4%) than females (Doran, 1993), the variation in the level of knee flexion/extension between sexes have not been previously described. Thus, if trabecular morphology reflects variation in the level of knee flexion/extension, there is no reason to predict these sex differences in the trabeculae of the knee in *Pan*. Similarly, we expect to find no significant differences in BV/TV and DA between female and male *Homo* as they are both obligate bipedal walkers.

4 | MATERIALS AND METHODS

4.1 | Study sample and scanning

4.1.1 | Study sample

The study sample consists of complete distal femora of *Homo sapiens* ($n = 26$ individuals), *Gorilla gorilla gorilla* ($n = 14$ individuals), *Pan troglodytes verus* ($n = 15$ individuals) and *Pongo* spp. ($n = 9$ individuals). Research involving non-human great apes plays a vital role in many anthropological and medical studies as their close phylogenetic relationship to humans makes them a useful model for reconstructing locomotor (and other) behaviours in hominin fossil record. The studied species were chosen as a representative sample of primates that use locomotor behaviours potentially found within the locomotor repertoires of fossil hominins. Details of the study sample are shown in Table 1. All great apes were wild born with no obvious signs of pathologies within their postcranial skeleton. The *Gorilla* sample is curated at the Powell-Cotton Museum in Birchington-on-Sea, UK, of which 13 individuals are from Cameroon and one is from the Democratic Republic of the Congo. The *Pan* sample is from the Taï Forest National Park, curated at the Max Planck Institute for Evolutionary Anthropology in Leipzig, Germany. The *Pongo* sample is from the Bavarian State Collection for Zoology in Munich, Germany and from the Natural History Museum in Berlin, Germany. Six individuals are *Pongo pygmaeus*, two are *P. abelii* and the species of one individual is unknown. Fifteen individuals of our human sample are from the W.M. Bass femoral collection from the Forensic Anthropology Centre at the University of Tennessee, USA and originate from diverse post-industrial populations. Eleven individuals are crew members of the Mary Rose ship from early 16th century (Barker, 1992) curated at the Portsmouth Museum, Portsmouth, UK. The Mary Rose sample comprises young adult males and are considered to represent high activity levels (e.g. Scorrer et al., 2021; Stirland & Waldron, 1997). Both human samples showed no obvious signs of pathologies within their postcranial skeleton. For most of our sample (91%), we used the right distal femur. However, when it was not possible due to preservation or methodological issues (such as low resolution of the CT scan), the mirrored left distal femur was used.

4.1.2 | MicroCT scanning

All distal femora were scanned via high-resolution micro-computed tomography (microCT) using a BIR ACTIS 225/300, Diondo D3 or Skyscan 1172 scanner housed at the Department of Human Evolution, Max Planck Institute for Evolutionary Anthropology (Leipzig, Germany), a Phoenix Nanotom S – X-ray tomograph at the Department of Micro-CT Laboratory, Museum of Natural History (Berlin, Germany), a Nikon 225/XTH scanner at the Cambridge Biotomography Centre, University of Cambridge (Cambridge, UK) or with the Diondo D1 scanner at the Imaging Centre for Life Sciences at the University of Kent (Canterbury, UK). The scan parameters included acceleration voltages of 100–160 kV and 100–140 μA using a 0.2 to 0.5 mm copper or brass filter. Scan resolution ranged between 0.024 mm and 0.058 mm depending on the size of the bone (Table 1). Images were reconstructed as 16-bit TIFF stacks.

4.2 | Data processing and trabecular bone analysis

Each distal femur was rotated into a standard anatomical orientation and non-bone inclusions were removed from the scans in Avizo Lite 9.0.0 (Visualization Sciences Group, SAS) (Figure 2a). Scans were subsequently segmented using the medical image analysis (MIA) clustering method (Dunmore et al., 2018) (Figure 2b). This method requires the definition of a grid size, which was selected by measuring the thickness of the thickest trabeculae in a cross-section and selecting a slightly higher value for each individual. A maximum of three classes were used across all individuals. MIA allows more accurate separation of trabeculae and offers more flexibility to deal

TABLE 1 Sample composition and voxel size range.

			Sex		Voxel size (mm)	
Taxon	**Locomotor behaviour**	***N***	**Female**	**Male**	**Min**	**Max**
Homo sapiens (1.0 kya to present)	Bipedal	15	Unknown		0.030	0.037
Homo sapiens (Mary Rose)	Bipedal	11	0	11	0.030	0.037
Gorilla gorilla gorilla	Terrestrial knuckle-walker	14	7	8	0.048	0.058
Pan troglodytes verus	Arboreal/knuckle-walker	15	8	7	0.029	0.030
Pongo sp.	Arboreal/suspensory	9	7	2	0.027	0.030
Total		64				

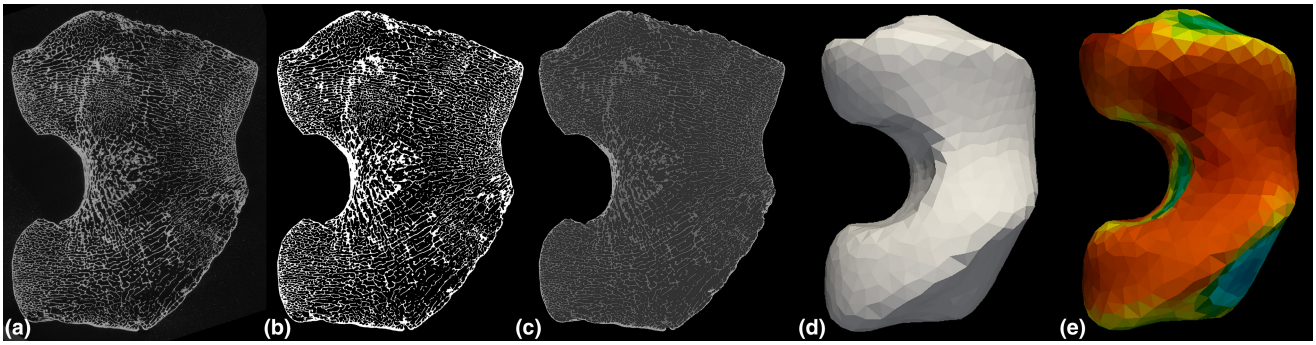

FIGURE 2 Processing steps of distal femur of a *Homo* specimen showing in inferior view. (a) Original high-res microCT image. (b) MicroCT image segmented by MIA (Dunmore et al., 2018). (c) MaskSeg defined by Medtool (Pahr & Zysset, 2009) showing the distinction between inner trabecular area and outer cortex. (d) Outer canonical atlas representing sample's mean size, position and external right distal femur morphology computed by cHMA (Bachmann et al., 2022). (e) Inner mesh representing rBV/TV distribution in human sample computed by cHMA (Bachmann et al., 2022).

with surrounding non-bone inclusions than other bone segmentation methods (Dunmore et al., 2018). The outer and inner layers of the cortex were defined using Medtool v 4.5 (www.dr-pahr.at/medtool), following published protocols (Gross et al., 2014; Pahr & Zysset, 2009). This involves morphological filters to fill the bone and use of a ray-casting method to isolate the external and internal edge of the cortex in 3D, resulting in a mask of the internal bone volume and outer cortex (Figure 2c).

4.2.1 | Canonical holistic morphometric analysis

A cHMA, combining HMA and statistical free-form deformation model (SDM), approach was used to analyse the patterns of trabecular bone distribution within whole epiphysis following published protocols (Bachmann et al., 2022). SDM operates on masked images of bones, where all images are registered onto a randomly chosen reference image using a similarity transform. All similarity transformations are then averaged and the centre of rotation is fixed. All images are then registered onto the aligned reference image and a free-form deformation is applied using a cubic B-spline transformation. The steps of registering and averaging can be repeated several times until the model has congregated. The last reference image is used as the canonical bone image for further steps of the analysis. The degree to which this may affect the results has been tested in Bachmann et al. (2022). In brief, cHMA creates a canonical bone from all the samples and then registers all samples onto that canonical bone. To create a canonical bone, we used 15 humans, 14 gorillas, 15 chimpanzees and 9 orangutan individuals to create canonical bone representing all species as much as possible. The canonical bone refers to the mean meshwork of bones formed from all the studied samples. All left-sided femora were mirrored in Avizo Lite 9.0.0 (Visualization Sciences Group, SAS) to resemble right-sided femora. All bones were then aligned into a mean position by translation and rotation in the image space and scaled to the mean bone size. Then, an SDM (Rueckert et al., 2003; Steiner et al., 2021) was used to create a canonical bone in 3D space representing the sample's mean internal and external bone morphology (in our case morphology of right distal femur) (Figure 2d). To produce the canonical atlas of the internal bone, the internal volume of each individual bone is used (Figure 2e). The canonical bone registration was run in Python 3.7.10, while required pre- and post-processing steps were performed in Medtool v 4.5 (www.dr-pahr.at/medtool). A 3D rectangular background grid with a grid size of 2.5 mm was built around each individual segmented volume and a sampling sphere (VOI) of 5 mm in diameter was used to measure BV/TV and DA across the entire bone in Medtool. Once these trabecular quantities were interpolated onto individual meshes, the meshes were deformed to the canonical mesh to allow for homologous volumetric comparisons.

DA was calculated using the mean intercept length method (Odgaard et al., 1997; Whitehouse, 1974). The value of DA is zero if the minor and major orientations are of equal magnitude, i.e. isotropic, and is one if the minor and major orientations are maximal different, i.e. anisotropic. Three-dimensional tetrahedral meshes of all specimens were created with CGAL 4.4 (CGAL, Computational Geometry, https://www.cgal.org), using the segmented trabecular structure and a characteristic mesh size of 3 mm. The morphometric values at each node of the background grid were then interpolated to the tetrahedral elements (back onto the canonical mesh) and the resulting BV/TV and DA distribution maps were visualized using Paraview 4.8.2 (Ahrens et al., 2005). Since data were collected from the canonical mesh, the datum collected at each node in the 3D grid is homologous between individuals. The BV/TV value for each mesh element was used to calculate the mean BV/TV for each individual. To compensate for potential systematic differences between selected taxa and to analyse bone volume distribution while controlling the magnitude, the BV/TV of each tetrahedron was divided by the overall average for that individual to give a measure of relative bone volume (rBV/TV). rBV/TV demonstrates where bone volume has increased or decreased relative to the mean allowing for comparisons between individuals and species that may differ in absolute BV/TV (Dunmore et al., 2019; Sukhdeo et al., 2020).

Femoral insertions of cruciate and collateral ligaments and of gastrocnemius muscle were located in the canonical distal femur shape (thus hereafter, just 'presumed insertions') based on their anatomical location for each studied species. Trabecular distribution under all ligament and muscle attachments of each individual was checked using the HMA of Medtool.

4.3 | Statistical analysis

All quantitative comparisons of measured variables and statistical analyses were conducted on the data generated from cHMA (Bachmann et al., 2022). All specimens have the same number of tetrahedral elements and the same topology. Only the position of the vertices changes. Thus, homology is accounted for by the topology of the canonical mesh and the tetrahedral elements of each specimen can be considered geometrically homologous (Bachmann et al., 2022). To analyse the distribution of trabecular bone in each species, principal component analyses (PCA) were run, creating two PCA models for rBV/TV and DA separately using the scalars associated with tetrahedral elements (including the geometry) of the canonical mesh as an input variable. This allows for visual comparison of the differences in genus-specific rBV/TV and DA patterns in distal femur. To demonstrate the loadings of each PC, we chose three standard deviations to represent 99.7% of the available variation. All values of the trabecular volumes were coloured by the signed loadings at three standard deviations of each principal component and thresholded at the 70th percentile of the rBV/TV or DA range. All PCA plots were done in R v3.4.1 using the rgl package (R Core Team, 2017). To explore if inter-specific allometry is driving species separation on PC1 of rBV/TV in our results, i.e. the potential that *Gorilla* has a different trabecular distribution because they have a larger body mass than *Pan*, we ran a regression of PC1 on 'bone volume' in all studied individuals (Figure S8). To explore potential intra-specific allometry, we ran a regression of PC1 on bone volume for each taxon separately (Figures S9–S11). We measured 3D bone size as the solid volume of the whole object, here the distal femur (as all femora were cut at a homologous location). This whole 'bone volume' (note this is not BV/TV in any sense) was measured for each of our individuals as a proxy for individual size. PC1 (as our sample species separate on PC1) could then be regressed on this bone volume.

5 | RESULTS

5.1 | Mean species trabecular bone distribution

5.1.1 | Relative bone volume in distal femur

Patellar surface and femoral condyles

In *Homo*, high rBV/TV (indicating the highest 30% of rBV/TV values, the regions assumed to be loaded the most) is concentrated in the posteroinferior volumes of both condyles, with higher values in the lateral condyle and on the patellar articular surface of the femur (Figure 3). In *Gorilla*, higher rBV/TV is found to extend from the inferior margin of the patellar articulation to the posterosuperior region of both condyles, again with higher values in the lateral condyle. *Gorilla* lacks trabecular concentration at the anterior regions of both condyles (i.e. regions assumed to be loaded in an extended knee). Posterosuperior and posteroinferior regions of both condyles exhibit lower rBV/TV concentrations in the deeper trabecular network of *Gorilla* and are evenly distributed between medial and lateral condyles compared to *Homo* (Figure 3). *Pan* exhibits a similar, but more spatially homogenous, rBV/TV distribution between the medial and lateral condyles as *Gorilla*. In *Pan*, rBV/TV is low in the anterior regions of both condyles as well; the low rBV/TV extends almost to the posteroinferior part of medial condyle, which differs from the pattern found in *Gorilla* (Figure 3). The most homogenous rBV/TV concentration is found in *Pongo*, with, again, low rBV/TV in anterior regions of both condyles. In *Pongo*, as in *Pan*, low rBV/TV almost reaches the posteroinferior part of medial condyle, however, the posteroinferior region of lateral condyle exhibits higher rBV/TV values compared to *Pan* (Figure 3).

Femoral insertions of cruciate and collateral ligaments

Note, even though approximate positions of ligaments and tendon insertion sites are well-known in humans and, to a lesser extent, great apes, the locations are necessarily artificial on the canonical models used in our study. Therefore, we state 'presumed' location to reflect our qualitative assessment of these insertions sites when interpreting the colour maps.

Homo exhibits high rBV/TV in the presumed insertions of cruciate ligaments, particularly for the posterior cruciate ligament in which high rBV/TV reaches to the middle of medial condyle (Figure 4). However, compared to medial condyle, rBV/TV under the anterior cruciate ligament does not penetrate as deeply into the trabecular network in lateral condyle (Figure 4). *Gorilla* also exhibits high rBV/TV in the presumed insertions of the cruciate ligaments, though not to the same degree as seen in *Homo*. rBV/TV under either cruciate insertion does not extend deeply into the epiphysis in *Gorilla* (Figure 4). *Pan* and *Pongo* show higher rBV/TV under the presumed insertions of both the posterior (medial condyle) and anterior (lateral condyle) cruciate ligaments than in *Gorilla*. rBV/TV under both insertions extends deeper into the epiphyses in *Pan* and *Pongo* compared to *Gorilla* or *Homo* (Figure 4) and in both taxa, rBV/TV under the posterior cruciate ligament extends deeper compared to that of the anterior cruciate ligament, particularly in *Pongo* (Figure 4).

High rBV/TV concentrations under the presumed insertions of collateral ligaments are present in all taxa. In *Homo*, the lateral epicondyle shows higher rBV/TV than the medial epicondyle. However, in neither case does the rBV/TV concentration extend deeply into the epiphysis (Figure 5). In great apes, relatively higher concentrations of rBV/TV are present under the medial epicondyle and the concentration within the lateral and medial epicondyles is more similar and extends slightly

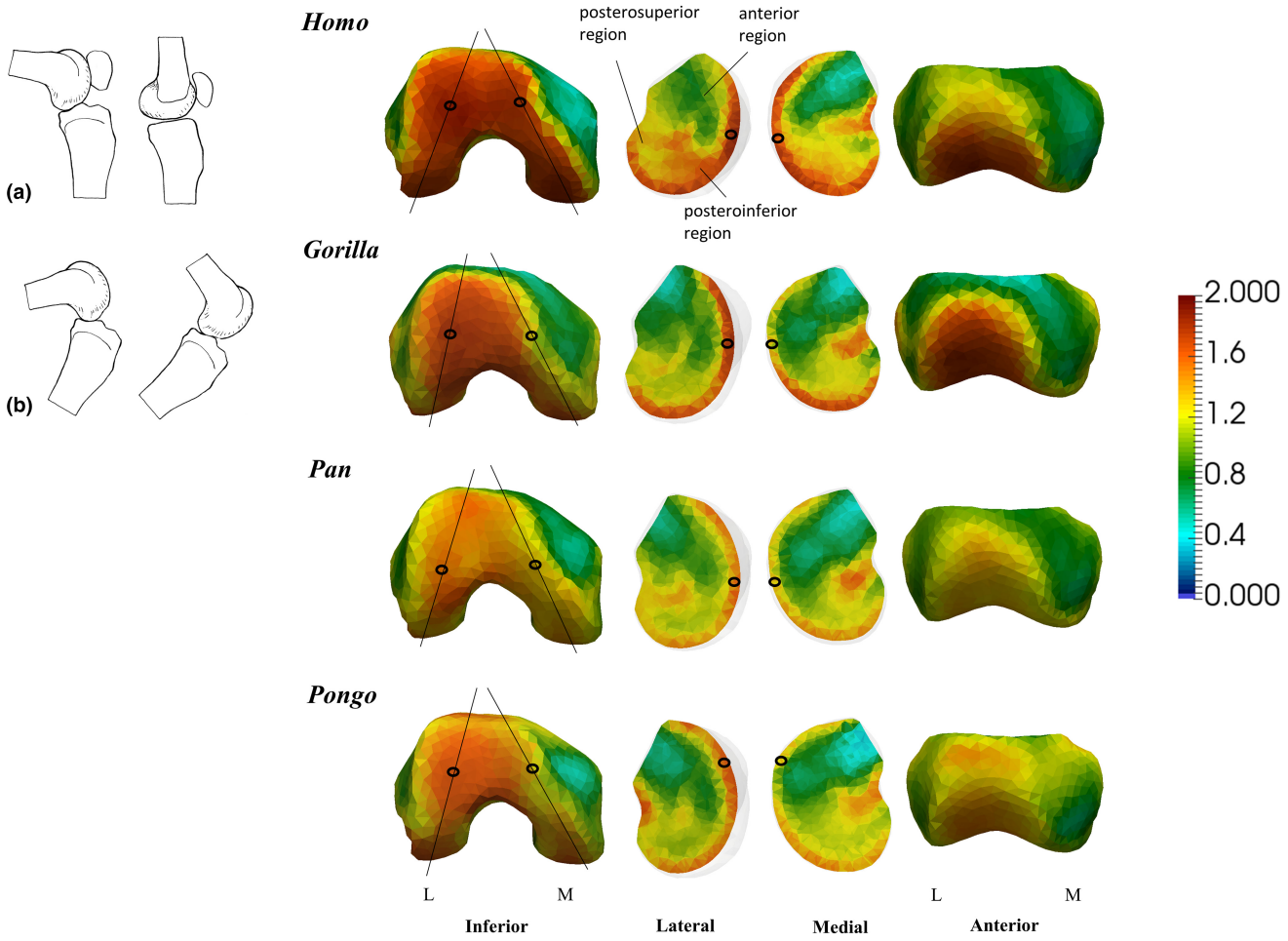

FIGURE 3 Species mean models of rBV/TV distribution in the patellar articular surface and femoral condyles of the distal femur of *Homo*, *Gorilla*, *Pan* and *Pongo*. Vertical lines through the inferior view mean models show where the slices are positioned. Cross sections were positioned in the middle of lateral and medial condyle. (a) Approximate patellar and condyle position during flexed (90°) and extended knee position in humans in medial view; (b) approximate condyle position during flexed and extended knee position in great apes. L, lateral; M, medial.

deeper into the epiphysis (especially in the region of the presumed medial collateral ligament insertion) compared to *Homo* (Figure 5).

Femoral insertions of gastrocnemius muscle

When looking at the posterior view of distal femur, high rBV/TV concentrations under the presumed insertions of gastrocnemius muscle are present in all taxa. In all taxa, the concentration under the presumed medial head goes deep inside the medial condyle; however, its presumed lateral head (with the highest values in *Pongo*) does not extend as deeply, especially in *Gorilla* (Figure 6). We found the most homogenous distribution under both presumed insertions of gastrocnemius in *Pan* and *Pongo*, but with lower values in *Pan* (Figure 6).

5.1.2 | Degree of anisotropy in the distal femur

Patellar surface, femoral condyles and femoral insertions of gastrocnemius muscle

The *Homo* mean distribution shows more anisotropic values in the posterosuperior/inferior regions of both condyles and under the patellar surface, with higher DA values in the lateral condyle (Figure 7). In *Gorilla*, DA is higher under the patellar surface on its medial side and more isotropic above the intercondylar fossa. Posterior regions of the *Gorilla* medial condyle are more anisotropic compared to posterior regions of lateral condyle. This pattern in the condyles is also found in *Pan* and *Pongo*, but posterior regions of lateral condyle are more anisotropic compared to that of *Gorilla* (Figure 7). The patellar surface of *Pan* shows more isotropic DA in the middle than on its medial or lateral side. This pattern is even more visible in *Homo* where DA values on the medial and lateral sides of patellar surface are even higher (Figure 7). *Pongo* exhibits a more homogenous distribution of moderate DA values; the most anisotropic values are in the posterior region of medial condyle and under the presumed insertions of cruciate ligaments relative to the patellar surface. In *Pongo*, DA values in both condyles are more homogenous compared to *Pan* (Figure 7). All taxa showed high DA values at the presumed insertions of gastrocnemius muscle (Figure 7).

Segmented images of each individual can be linked with the anisotropic/isotropic parts of the bone presented in the mean colour

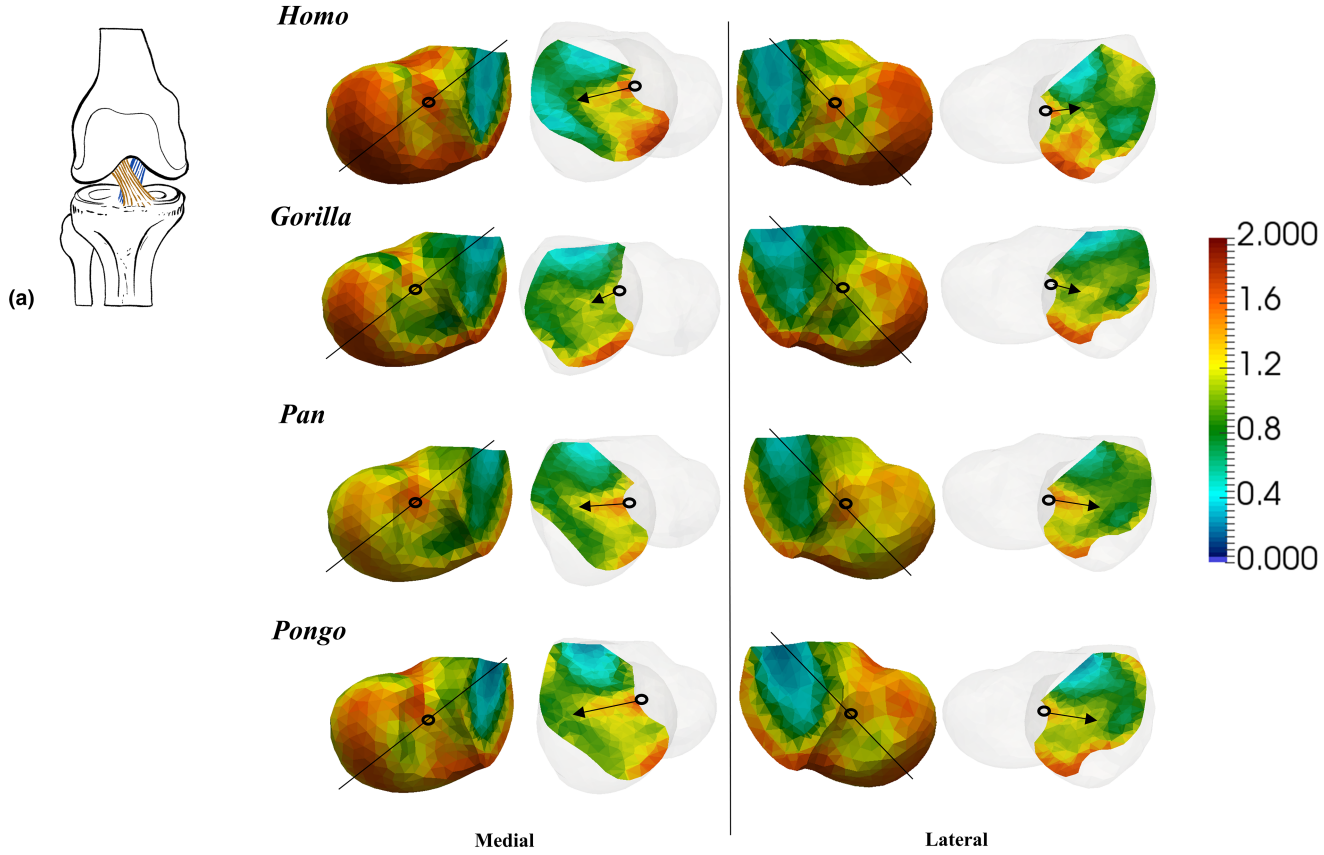

FIGURE 4 Species mean models of rBV/TV distribution under the presumed insertion of cruciate ligaments of the distal femur of *Homo*, *Gorilla*, *Pan* and *Pongo*. Vertical lines through the medial and lateral mean models show where the slices are positioned. Cross sections were positioned in the middle of presumed insertions of cruciate ligaments. (a) Anterior cruciate ligaments during neutral knee position in the anterior view.

maps. Figure 8 shows one representative individual of *Homo* and *Gorilla* to demonstrate the pattern of high DA in the lateral condyle, and beneath the presumed medial head of gastrocnemius muscle in *Homo* (Figure 8a), as well as high DA in the medial condyle of *Gorilla* (Figure 8b). Note that the signal within each individual might not be strong, while the mean colour maps are a representation of all individuals within a specific taxon.

5.2 | Principle component analyses

Figure 9 presents the results of a principal component analysis of rBV/TV distribution in the distal femur. PC1 explained 21.4% of the variation in rBV/TV values at each mesh cell. PC1 separates *Homo* from great apes with positive PC1 scores associated with higher rBV/TV on the patellar surface of the femur and on its medial distal articular surface. Negative PC1 scores, associated with the great apes, are associated with higher rBV/TV under the medial and lateral epicondyles and in the posteroinferior region of lateral condyle. PC2 accounted for 9.1% of the variation in rBV/TV values and separates *Pan* and *Pongo* from *Gorilla*. Positive PC2 distinguishes *Gorilla* not only due to a different pattern under the patellar surface but also especially due to higher rBV/TV under both presumed insertions of gastrocnemius muscle. Negative PC2 separates *Pan* and *Pongo* mostly due to their higher lateral loading of patellar surface and the rBV/TV concentration in the anterior part of lateral condyle. However, because all taxa share a similar rBV/TV concentration on the patellar surface (Figure 3), the separation on PC2 more likely reflects the low rBV/TV concentration at the presumed insertions of gastrocnemius muscle in *Pan* and *Pongo* compared to *Gorilla*.

The PCA of DA values reveals separation among the different taxa in distal femur (Figure 10). PC1 accounted for 22.2% of the variation in DA values. Positive PC1 separates *Homo*, with highly aligned trabeculae on the lateral side of the patellar surface, in the presumed insertion of the lateral head of gastrocnemius and by higher DA in the posteroinferior region of the lateral condyle (Figure 10). Negative PC1 separates great apes, with high DA under the presumed insertions of vastus lateralis and medialis, under the presumed insertion of medial head of gastrocnemius, and in the medial condyle, where we see highly align trabeculae in posterosuperior/inferior regions (Figure 10). PC2 explained 7.3% of the variation in DA values. Positive PC2 separates *Gorilla* and *Pan* from *Pongo* with highly aligned trabeculae where vastus lateralis and medialis cross the femur. In contrast, negative PC2 separates *Pongo* from *Gorilla* and *Pan* by high DA in the posterosuperior/inferior regions of lateral and medial condyles (Figure 10).

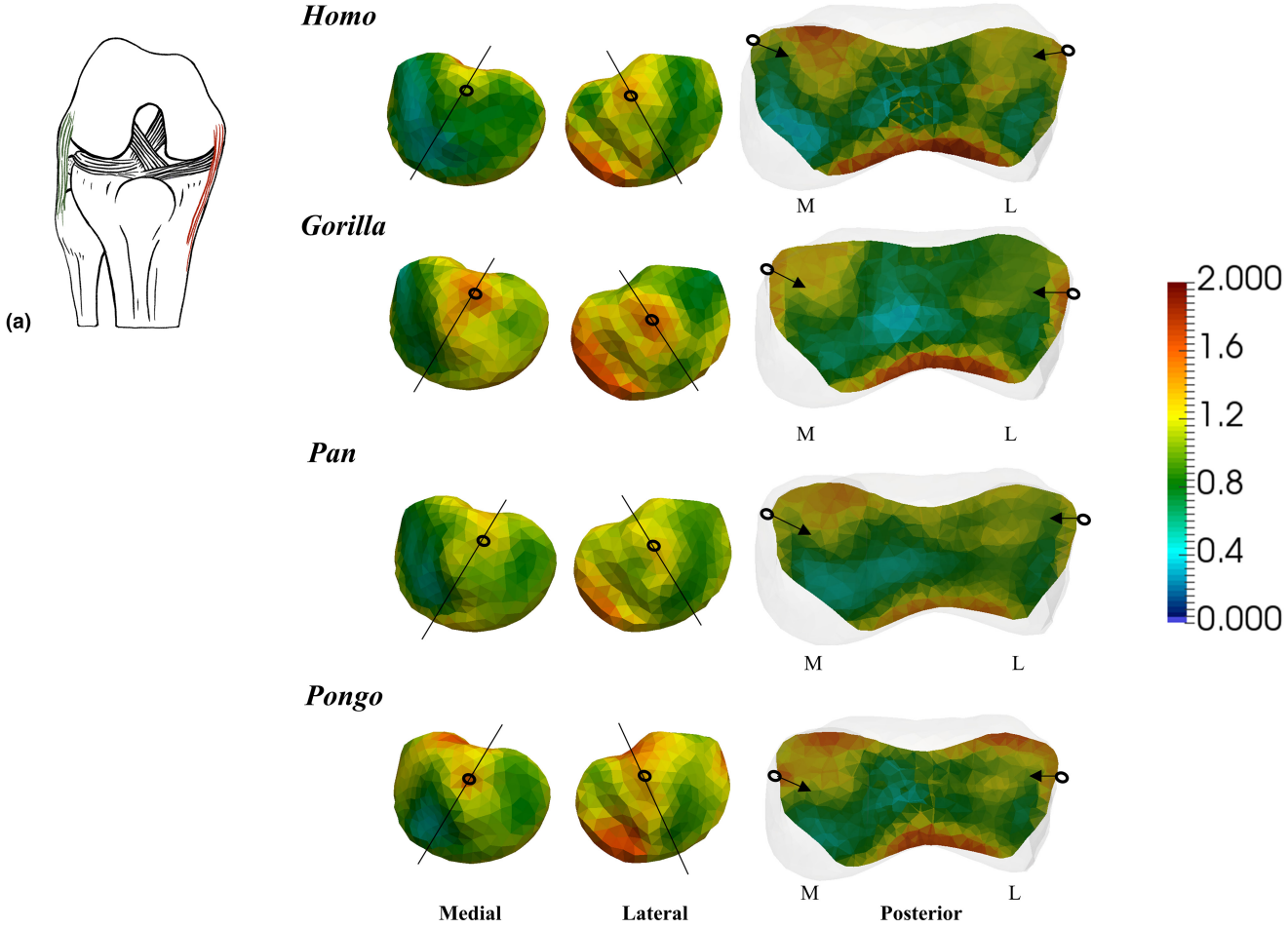

FIGURE 5 Species mean models of rBV/TV distribution under the presumed insertions of collateral ligaments of the distal femur of *Homo*, *Gorilla*, *Pan* and *Pongo*. Vertical lines through the medial and lateral mean models show where the slices are positioned. Cross sections were positioned in the middle of presumed insertions of collateral ligaments. (a) Lateral collateral ligaments attachments. L, lateral; M, medial.

5.3 | Trabecular bone distribution in *Homo*, *Gorilla* and *Pan* by sex

Figure 11a shows PCA of rBV/TV distribution in *Gorilla*. Female and male *Gorilla* do not separate on PC1 (explaining 15.5% of the variation). PC2 accounted for 14.6% of the variation in rBV/TV values. Thresholded mean models show that females separate from males (positive PC2) due to higher rBV/TV on the lateral side of patellar surface and on the articular surface of medial and lateral condyles. Female *Gorilla* also show higher rBV/TV in the lateral epicondyle and in the posteroinferior region of lateral condyle compared to males. In contrast, in male *Gorilla*, high rBV/TV values extend to the medial side of patellar surface and are more homogeneous across the patellar surface. Figure 11b shows PCA of DA distribution in *Gorilla*. PC1 accounted for 22.3% of the variation in DA values. Positive PC1 distinguishes *Gorilla* males due to higher DA values under the presumed insertions of vastus lateralis and medialis muscles and negative PC1 distinguishes females due to higher values inside the medial condyle and under the presumed insertion of medial head of gastrocnemius (Figure 11b). We found no separation in rBV/TV and DA distribution between the sexes in *Pan* (Figure 11a,b).

Figure S7 shows that the relative PC1 positions for rBV/TV (explaining 21.4% of the variation) and PC1 positions for DA (explaining 22.2% variation) remained constant when we divided the *Homo* sample by population (Mary Rose sample is represented by 11 male individuals) for a PCA. Note that we could have no test sex differences across whole human sample as sex is known only for 11 (male) of the 26 individuals.

5.4 | Allometry in our sample

We found no significant relationship between PC1 and bone volume (R^2 =0.002, p=0.890) across our sample (Figure S8). We found no significant relationship (R^2 =0.007, p=0.740) in *Gorilla* (sexes pooled; Figure S9). However, male *Gorilla* showed a stronger negative, if non-significant, relationship (R^2 =0.490, p=0.110) compared to females (R^2 =0.090, p=0.710) (Figure S9). We found a significant negative relationship (R^2 =0.292, p=0.011) in *Pan*,

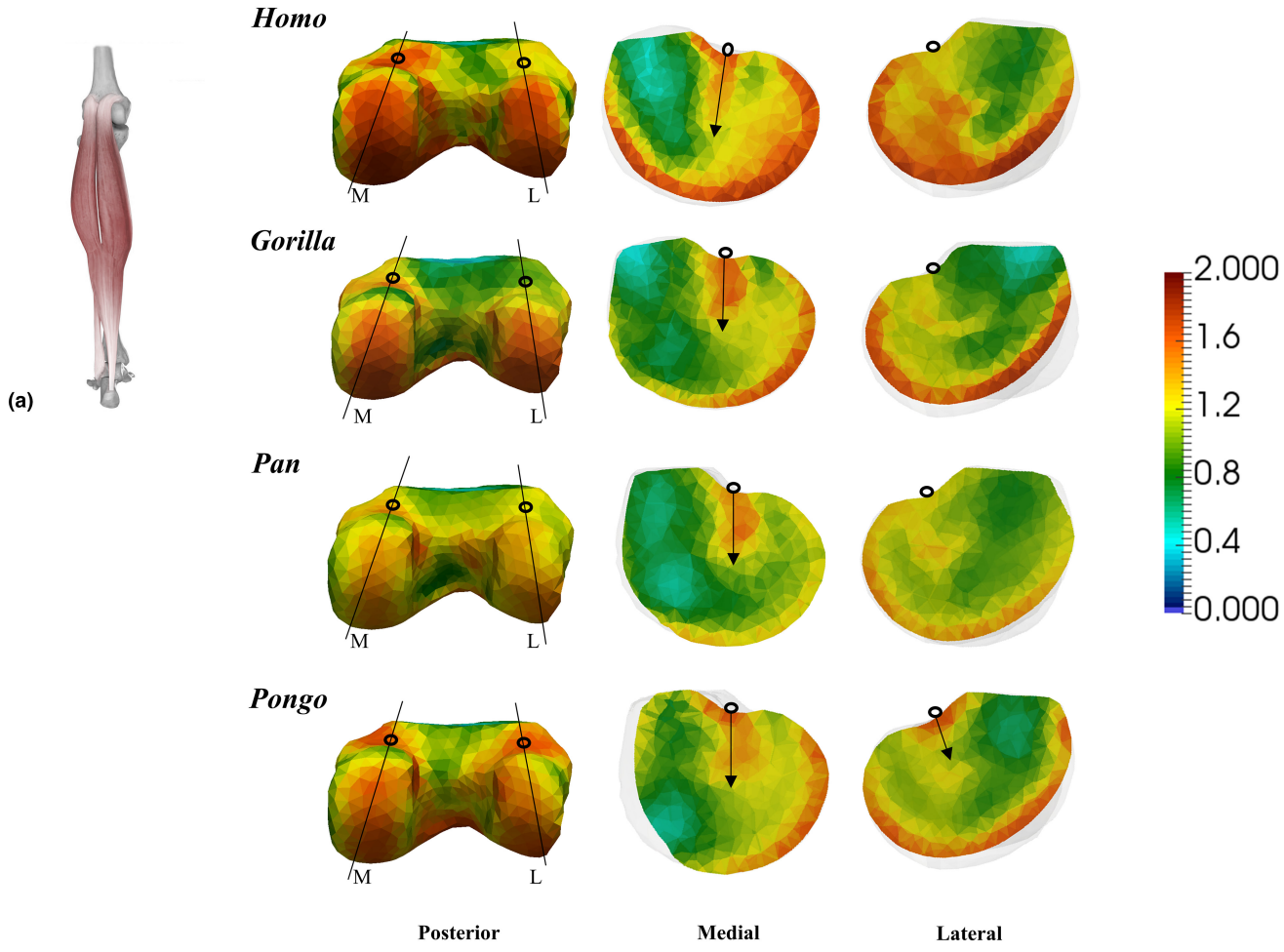

FIGURE 6 Species mean models of rBV/TV distribution under the presumed gastrocnemius muscle attachments of the distal femur of *Homo*, *Gorilla*, *Pan* and *Pongo*. Vertical lines through the posterior mean models show where the slices are positioned. Cross sections were positioned in the middle of presumed gastrocnemius attachments. (a) Gastrocnemius attachments. L, lateral; M, medial.

but no significant relationship within each sex, though females had a stronger relationship (R^2 =0.436, p=0.059) than males (R^2 =0.212, p=0.069) (Figure S10). Finally, as our human sample is predominantly male, we explored potential allometric differences between populations. We found no significant relationship across all humans (R^2 =0.058, p=0.170) and neither in the sedentary population (R^2 =0.221, p=0.280) or the active population (R^2 =0.012, p=1.000) (Figure S11).

6 | DISCUSSION

This study investigated trabecular variation in the distal femur of great apes and *Homo*. We expected trabecular architecture to differ based on different types of locomotion and predicted differences in habitual knee joint postures in extant hominid taxa. Also, we expected to find differences in trabecular architecture between female and male *Gorilla*, due to higher female arboreality, and to find no sex differences within *Pan* and *Homo*. We found general support for all our predictions.

6.1 | Trabecular bone structure of the distal femur in human bipedal walking

We predicted that *Homo* would be significantly different from other great apes in having a trabecular structure of the distal femur that reflected habitual use of extended knee postures during bipedalism. This prediction was supported. High rBV/TV values in posteroinferior regions of both condyles (Figure 3) were consistent with the extended knee postures during all gait phases of human walking. High rBV/TV concentration in lateral condyle (Figure 3) was consistent with the resistance, provided by the quadriceps and gastrocnemius muscles and medial collateral ligament, of the knee adduction moment (when the tibia medially rotates on the knee joint in the frontal plane) and with valgus knee postures (Nordin & Frankel, 2001; Racic et al., 2009). High rBV/TV concentration in the lateral condyle is consistent with human bipedal heel strike and subsequently transferring weight from the lateral side of the foot to the medial side (Elftman & Manter, 1935; Napier, 1967). The distinct rBV/TV distribution in patellar surface in *Homo* compared to great apes (Figure 3) most likely reflected a more convex trochlea, such

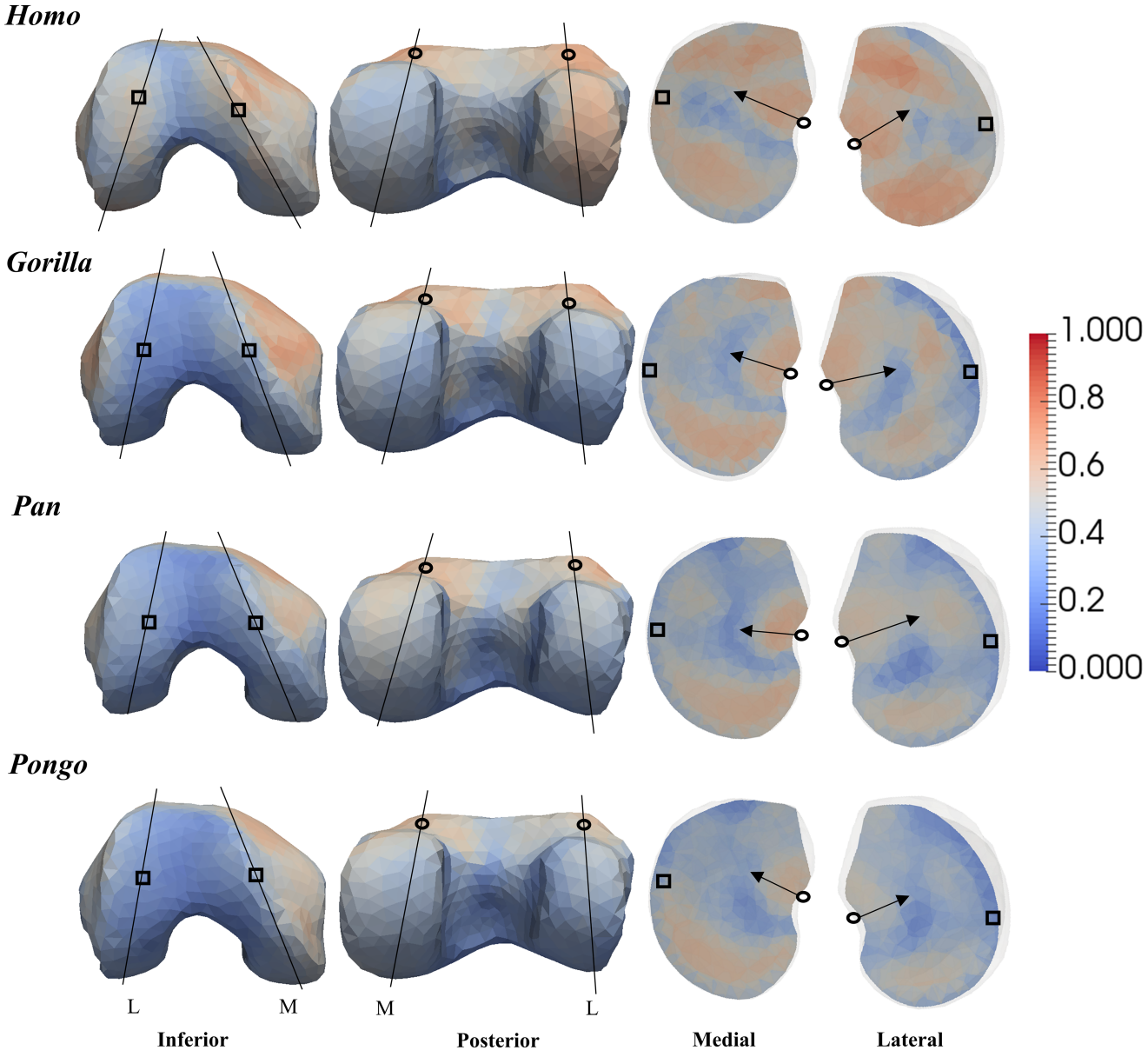

FIGURE 7 Species mean models of DA distribution in the patellar articular surface (marked with square) and in the presumed insertions of gastrocnemius muscle attachments (marked with circle) of the distal femur of *Homo*, *Gorilla*, *Pan* and *Pongo*. Vertical lines through the inferior view mean models show where the slices are positioned. Cross sections were positioned in the middle of lateral and medial condyle. L, lateral; M, medial.

loading is distributed, with flatter trochlea, more evenly across the patellar articular surface in great apes. We found high rBV/TV values on the patellar articular surface being extended more mediolaterally, reflecting the patella's more extensive articulation with the lateral part of the trochlea than with its medial part (Figure 3). Moreover, high rBV/TV was also found beneath the presumed insertions of gastrocnemius and those of the femoral ligaments (Figures 3–6) (see next). The human distal femur was more anisotropic posterosuperiorly/inferiorly in both condyles and under the patellar articular surface than in great apes (Figure 7). This DA pattern was also consistent with what we would expect from loading during human's stereotypical extended knee postures. Furthermore, high DA was also found beneath the presumed insertions of gastrocnemius and vastus lateralis and medialis muscles (Figures 7, 8; Figure S5) (see next). Overall, the trabecular distribution patterns found in our human sample are consistent with variation in trabecular structure found in previous studies of the proximal (Cazenave et al., 2019; Georgiou et al., 2019; Georgiou et al., 2020; Ruff et al., 2013; Ryan & Ketcham, 2002; Ryan & Walker, 2010; Volpato et al., 2008) and distal (Georgiou et al., 2018; Sylvester & Terhune, 2017) femur and with our current biomechanical understanding of human walking cycle (Alexander, 1991, 2004; Elftman & Manter, 1935; Javois et al., 2009; Landis & Karnick, 2006; Napier, 1967; Organ & Ward, 2006; Sylvester & Pfisterer, 2012; Tardieu, 1999).

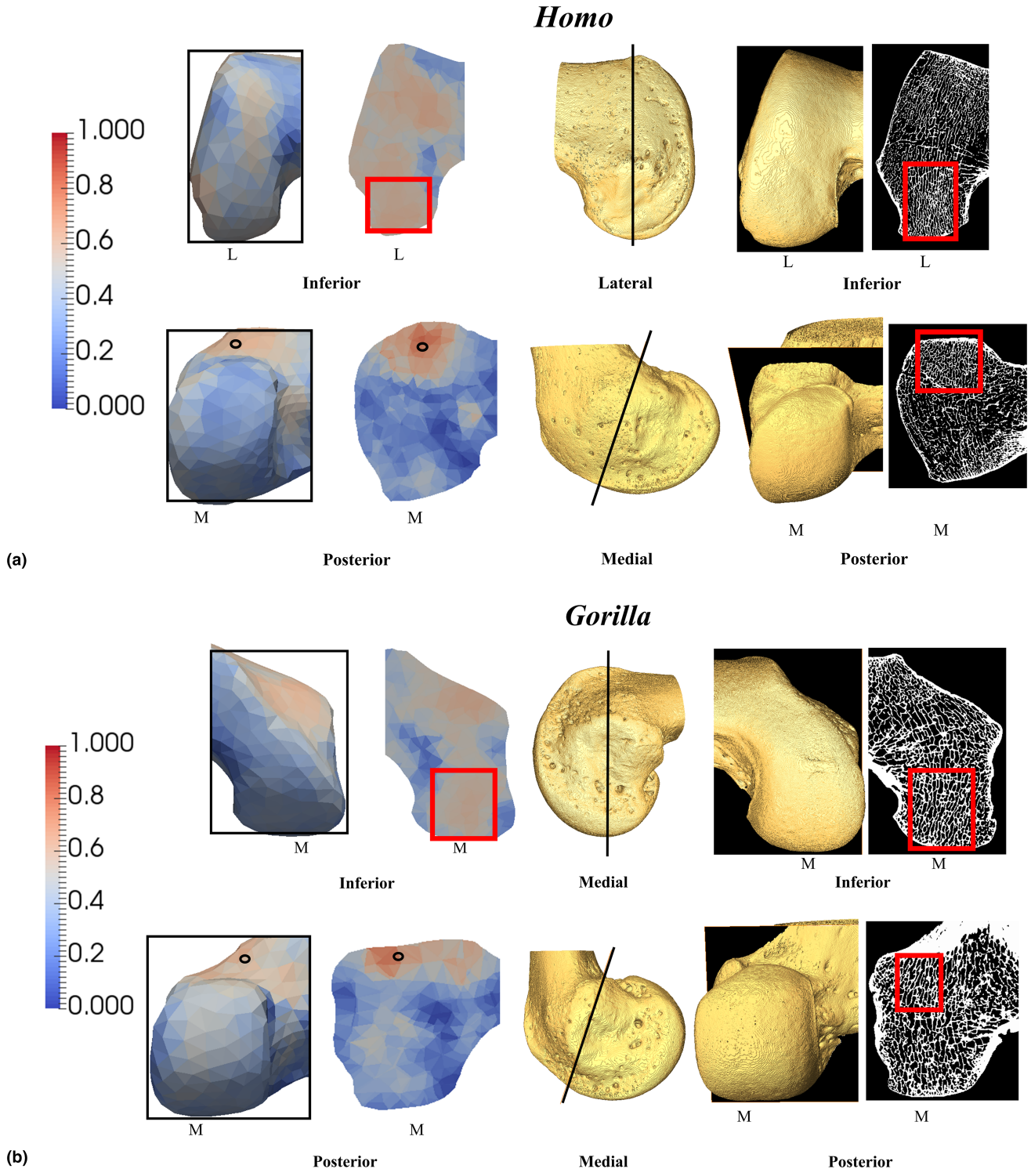

FIGURE 8 HMA and segmented models showing high DA concentration in the lateral/medial condyle and under the presumed insertions of gastrocnemius muscle attachments (marked with circle) of the distal femur of (a) *Homo* and (b) *Gorilla* individual. Vertical lines/squares show where the slices are positioned. L, lateral; M, medial.

6.2 | African ape trabecular bone structure and locomotor behaviour

We predicted that *Pan* and *Gorilla* would significantly differ from *Homo* and *Pongo*, but not from each other, in having a trabecular structure of the distal femur that reflected habitual use of a flexed knee posture during terrestrial and arboreal locomotion. This prediction was not fully supported. Compared to higher rBV/TV in the inferior patellar articulation in *Homo*, we found rBV/TV concentration posterosuperiorly in the condyles and mediolaterally

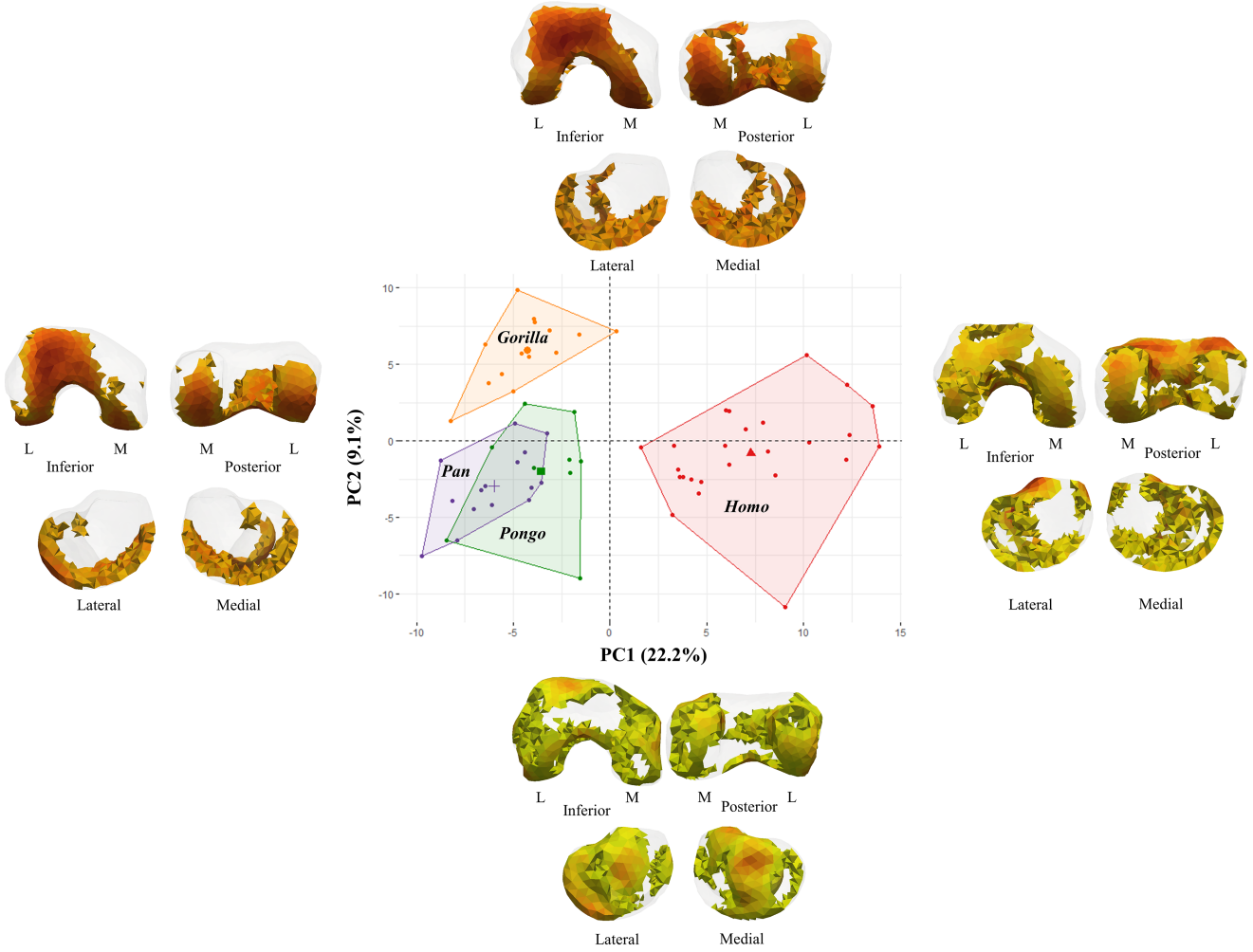

FIGURE 9 PCA of rBV/TV distribution in the distal femur of *Homo*, *Gorilla*, *Pan* and *Pongo* showing separation among studied taxa. Thresholding models represent high 30% of the range of rBV/TV values for negative and positive PCAs. Models demonstrate the highest loading causing the separation between humans (negative PC1 − 3SD) and great apes (positive PC1 + 3SD); between *Pongo*, *Pan* (negative PC2 − 3SD) and *Gorilla* (positive PC2 + 3SD). L, lateral; M, medial.

on the patellar articulation in African apes (Figure 3). This trabecular pattern is consistent with higher and more uniaxial loading of the distal femur in a flexed knee posture, which is used during quadrupedal knuckle-walking and vertical climbing in both taxa (D'Août et al., 2002, 2004; Georgiou et al., 2020; Isler, 2005). However, we also found some trabecular patterns that separate *Gorilla* from *Pan* (Figures 3, 9). The more homogenous rBV/TV distribution between and within both condyles of distal femur in *Pan* compared to *Gorilla* (Figure 3) may reflect the more variable knee loading that has been documented during climbing in captive *Pan* (Isler, 2005). However, the trabecular pattern under the patellar articular surface in *Pan* (Figure 9) suggested an opposite functional signal, with higher lateral loading of the patellar articular surface, which might be related to the quadriceps muscles that are active regardless of climbing posture and thus always pulling on the patella in the same way. Moreover, high rBV/TV was also found beneath the presumed insertions of gastrocnemius and under the presumed insertions of femoral ligaments (Figures 4–6) (see next). *Gorilla* and *Pan* both displayed the highest DA in the posteroinferior/superior regions of (especially) the medial condyle (Figure 7), which is again consistent with their stereotypically flexed knee postures and higher loading of medial knee compartment (Ankel-Simons, 2010; Crompton et al., 2008; D'Août et al., 2004; Georgiou et al., 2018; Isler, 2005; Kozma et al., 2018; Lee et al., 2012; Pontzer et al., 2009). High DA was also found at the presumed insertion sites of muscle tendons (Figures 7, 8; Figure S5) (see next).

6.3 | *Pongo* trabecular bone structure and locomotor behaviour

We predicted that *Pongo* would exhibit the most homogenous trabecular distribution across the distal femur compared to other apes due to their more variable knee joint postures during locomotion. This prediction was not fully supported. Even though *Pongo* trabecular structure was found to be quite homogenous, *Pan* also exhibited

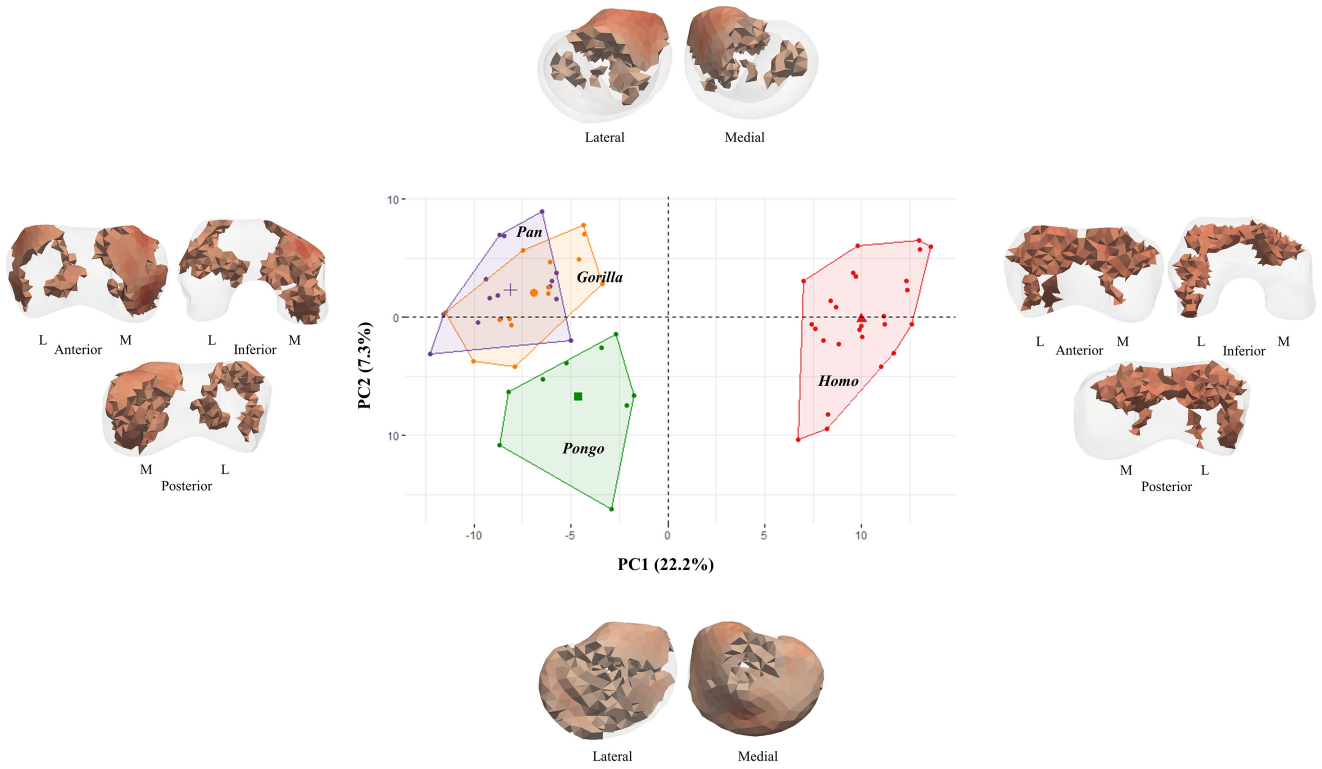

FIGURE 10 PCA of DA distribution in the distal femur of *Homo*, *Gorilla*, *Pan* and *Pongo* showing separation among studied taxa. Thresholding models represent high 30% of the range of DA values for negative and positive PCAs. Models demonstrate the highest loading causing the separation between humans (positive PC1 + 3SD) and great apes (negative PC1 − 3SD); between *Gorilla*, *Pan* (positive PC2 + 3SD) and *Pongo* (negative PC2 − 3SD). L, lateral; M, medial.

a similar pattern (Figure 3). Like African apes, *Pongo* did not show trabecular concentrations at the anterior regions of both condyles (Figure 3). *Pongo* shared with *Pan* low rBV/TV in the posteroinferior region of the medial condyle but had higher rBV/TV in the posteroinferior region of the lateral condyle (Figure 3). This pattern may suggest higher lateral loading during knee extension or higher degree of knee extension in *Pongo* compared with *Pan*. Posterior regions of both condyles were anisotropic as in African apes in *Pongo*. Moreover, we found rBV/TV concentration beneath the presumed insertions of gastrocnemius and under the presumed insertions of femoral ligaments (Figures 4–6) (see next). As in *Homo* and African apes, highly aligned trabeculae were also found at the presumed insertion sites of muscle tendons (Figures 7; Figure S5) (see next). *Pongo* is thought to have the most variable knee range of motion (Payne et al., 2006; Pina et al., 2014; Zihlman et al., 2011), together, these results are consistent with the highly mobile knee joint (Morbeck and Zihlman, 1989) that enables more variable loading during a diverse locomotor repertoire (Cant, 1987; Thorpe 2009; Thorpe & Crompton, 2006; Thorpe et al., 2007).

6.4 | Sex differences in *Gorilla*

We predicted that female and male *Gorilla* would significantly differ from each other due to higher arboreality and/or more extended knee posture when climbing in females (e.g. Hammond, 2014; Isler, 2005). This prediction was supported. We found distinct sex differences in our *Gorilla* sample, with females showing higher rBV/TV concentration in the posterior regions of lateral condyle, laterally on patellar surface and medially above intercondylar fossa (Figure 11a). In contrast, *Gorilla* males had higher rBV/TV concentrations in the medial epicondyle (Figure 11a). This sex pattern could suggest that in females there is higher lateral knee compartment loading and/or a more extended knee posture, as previously discussed in some studies (Crompton et al., 2008; Isler, 2005; Kozma et al., 2018) compared to more flexed knee position and/or greater lateral knee rotation during extension in males. Lateral knee rotation during extension has been previously discussed in *Pan* (Lovejoy, 2007), but it is currently unknown if this rotation is also found in *Gorilla*. Additionally, it is possible that low degree of extension (more common in males) is compensated for by the lateral rotation, but when the knee is highly extended, there may be more medial knee rotation (more common in females). Alternatively, when the knee flexes, posterior regions of the femoral condyles are expected to resist continuous compression, resulting in denser bone in these regions (Georgiou et al., 2018; Sylvester & Terhune, 2017). Thus, rBV/TV values potential higher increase in medial condyle compared to lateral condyle, as seen in our *Gorilla* male sample, could also suggest higher knee flexion in males compared to females. Moreover, we found females separating from males due to

FIGURE 11 PCA of rBV/TV and DA distribution in the distal femur of *Gorilla* and *Pan*. (a) PCA of rBV/TV distribution of *Gorilla* and *Pan* showing separation between sexes in *Gorilla* and no separation in *Pan*. (b) PCA of DA distribution of *Gorilla* and *Pan* showing separation between sexes in *Gorilla* and no separation in *Pan*. Thresholding models represent high 30% of the range of rBV/TV and DA values for negative and positive PCs. Models demonstrate the highest loading causing the separation between female and male gorillas. L, lateral; M, medial; *F*, female; *M*, male.

the higher anisotropy under both presumed insertions of gastrocnemius muscle (Figure 11b) (see next). However, the discussion of locomotor behaviour of lowland *Gorilla* is limited by lack of locomotor data in wild populations; with the exception of Remis (1994, 1995), all other locomotor studies derive from mountain gorillas (e.g. Doran, 1997; Thompson et al., 2018).

6.5 | Can trabecular structure underlying ligament/tendon attachments inform loading?

Our analysis also highlighted clear concentrations of rBV/TV at the presumed insertion sites of muscle tendons and knee joint ligaments (Figures 4–6) and high DA at the presumed insertion sites of muscle tendons in all taxa (Figures 7, 8; Figure S5). High rBV/TV values in the presumed insertions of cruciate ligaments illustrate that loading of these ligaments is resulting in modelling of underlying trabecular bone. Higher bone density at both cruciate ligaments insertion sites in all taxa (Figure 4) likely reflects the need to protect and stabilize the femur from dislocation throughout its range of motion. However, at both ligament insertion sites, *Pan* and *Pongo* showed higher trabecular density that extended deeper into the epiphysis compared with *Gorilla* (Figure 4), which may reflect more variable knee loading in the former. Potential support for this hypothesis would be more well-developed trabeculae under the cruciate ligament sites in female *Gorilla* compared to males, which we did find (Figure 11a). In addition, loading of the collateral ligaments also appears to stimulate increased rBV/TV under their insertion points in all taxa. Collateral ligaments, in theory, should be loose when the knee is flexed to allow more rotational movements, and tightened when the knee is extended. Here it seems they are equally loaded in African apes, which could suggest a certain degree of medial and lateral knee rotation when knee is not in full flexion (eventually when knee is extended). Lateral knee rotation during knee extension has been previously discussed in *Pan*. However, this would imply higher bone density under the insertion of medial collateral ligament compared to lateral collateral ligament. The separation of *Homo* from great apes was driven primarily by differences in trabecular structure at both collateral ligament insertion sites (Figure 9), suggesting different loading when knee is in extension and/or flexion.

In humans, gastrocnemius is a complex muscle that is involved in running, jumping and other fast movements of the leg, and to a lesser degree in walking and standing (e.g. Huijing, 1985; Ishikawa et al., 2007; Maganaris, 2003; Muramatsu et al., 2001). rBV/TV distribution beneath the insertions of gastrocnemius in *Homo* could result from forceful extension of knee and/or the hip joint in our sample (Anderson & Pandy, 2001; Baltzopoulos, 1995; Georgiou et al., 2020; Hardt, 1978; Simpson & Pettit, 1997; Taylor et al., 2004; Zheng et al., 1998). The specific activation of this muscle during different locomotor and postural activities in *Homo* is not known (Ishikawa et al., 2007), but the highly aligned trabeculae in the presumed insertions of gastrocnemius suggest that this region of the bone is loaded frequently and in a similar direction. Although Stern Jr and Susman (1981) have not measured the activity of the gastrocnemius muscle, they found activation of the gluteus medius and, to a lesser extent, the gluteus superficialis muscles to be similar in African ape climbing as in humans during bipedality. Since gastrocnemius is in action during most of the hindlimb activities in *Homo* (Georgiou et al., 2018; Ishikawa et al., 2007; Lichtwark et al., 2007; Neptune et al., 2001), it is presumably actively involved during arboreal locomotion in African apes as well. It has been previously found that gastrocnemius muscle becomes an extensor at highly flexed postures of the knee (Goh et al., 2017). Both *Pan* and *Gorilla* are characterized by flexed knee postures during quadrupedalism (Finestone et al., 2018) and particularly during climbing (Crompton et al., 2008; D'Août et al., 2002; Isler, 2005; Kozma et al., 2018) and thus, we would not expect they would separate from each other based on both presumed gastrocnemius insertions. We suggest that this could be the case of either more robust quadriceps muscle in *Gorilla* (e.g. Zihlman et al., 2011) or this muscle is somehow involved more during locomotion in *Gorilla* compared to *Pan*. The separation of female *Gorilla* from male *Gorilla* due to the higher anisotropy under both presumed insertions of gastrocnemius muscle suggests more stereotypical loading of gastrocnemius muscle in females compared to males and that perhaps this muscle is more active during climbing, which female *Gorilla* are thought to do more frequently than males (Isler, 2005; Kozma et al., 2018). The high rBV/TV and DA values in both presumed insertions of gastrocnemius muscle in *Pongo* could be the result of the involvement of this muscle during suspension by the lower limbs, which is common in *Pongo* (Thorpe & Crompton, 2006).

We also found that *Gorilla* and *Pan* are distinguished from *Pongo*, and likewise male *Gorilla* from female *Gorilla*, in their much more aligned trabecular structure at the presumed insertions of vastus lateralis and medialis. In quadrupedal primates, vastus lateralis and medialis are pulled towards the joint as the knee is flexed, causing the moment arm to decrease with increasing flexion (Krevolin et al., 2004; Spoor & Van Leeuwen, 1992; Visser et al., 1990). Thus, this might be a result of higher knee flexion in African apes compared to *Pongo* and of higher knee flexion in male *Gorilla* compared to female *Gorilla*. However, it is not clear if this anisotropy is caused by the contraction of vastus medialis and lateralis or/and joint reaction forces experienced by the femoral condyles towards the shaft.

6.6 | Trabecular bone and body mass

Although current research on allometry has not yielded consistent results (e.g. Barak et al., 2011; Cotter et al., 2009; Doube et al., 2011; Ryan & Shaw, 2013), one of the factors affecting trabecular bone structure is body mass. Thus, comparative research incorporating taxa of variable body mass should consider the effects of allometry when interpreting biomechanical and behavioural signals (Ruff et al., 2006). As body size increases, the gravitational forces also increase and thus the loads imposed upon the joints are higher (Doube et al., 2011). As bones get longer, they tend to become more

robust in overall external shape (Doube et al., 2011). Altering any of several properties of trabecular bone such as its volume, thickness or number can be an effective way to resist increasing joint loads caused by increasing body mass (Currey, 2003; Doube et al., 2011). Trabecular thickness, spacing, connectivity and number have been shown to significantly correlate with body mass such that trabeculae are thinner, more widely spaced and more numerous in smaller mammals compared to larger mammals (e.g. Barak et al., 2013; Cotter et al., 2009; Doube et al., 2011; Ryan & Shaw, 2013; Saers et al., 2019). In contrast, BV/TV and DA show no significant correlation with body mass and are considered to be relatively constant across species of various sizes (Barak et al., 2013; Cotter et al., 2009; Doube et al., 2011; Ryan & Shaw, 2013). However, Barak et al. (2013) also noted that BV/TV can increase through different mechanisms depending on body mass; in humans (70 kg), BV/TV increased via increases in trabecular thickness, while in rodents (e.g. 40 g and orders of magnitude smaller), BV/TV increased via increases in trabecular number (Barak et al., 2013).

In our study, average body mass varies from 36 kg (female *Pongo*) to 170 kg (male *Gorilla*; Smith & Jungers, 1997) and previous studies of extant hominid trabecular bone structure confirm no significant allometric effect on the variables (BV/TV and DA) that we analysed (e.g. Barak et al., 2013; Cotter et al., 2009; Ryan & Shaw, 2013). We found no significant allometric relationship on inter-specific level across our sample and only a weak significant negative relationship in *Pan* (sexes pooled) on the intra-specific level. Thus, we consider allometry to have little to no effect on our results of rBV/TV distribution and species separation. However, future investigation on intra-specific allometric effects on larger samples of females and males within each taxon, particularly for highly sexually dimorphic taxa, would be interesting to explore in more detail.

6.7 | Limitations

There are some limitations to this study that should be acknowledged. First, the colour maps of DA show regions with high/low anisotropy, but do not show the direction in which the trabeculae are oriented (Figures 7, 8; Figures S3–S5). The technical limitation of cHMA is that vectors and tensors cannot (yet) be transformed into the canonical space. Thus, we did not quantitatively explore the direction of loading in the highly anisotropic parts of distal femur (especially under the presumed insertions of vastus lateralis and medialis tendons). We suggest that future studies of trabecular structure should explore difference in the direction of trabecular orientation in extant primates; this may provide more informed functional interpretations of how the ligaments and muscles are involved in knee movements during specific types of locomotion. In addition, our functional interpretations are also limited by a lack of kinetic and kinematic data of the knee in non-human great apes, and most notably in wild populations.

Second, our study also found that *Pongo* has the most homogenous trabecular distribution, which not only is expected but also may be the result of the conflation of two *Pongo* species. The difficulty in obtaining high-resolution CT scans of complete adult *Pongo* distal femur also resulted in a lower sample size for this group and thus we were not able to explore sex differences. Future analysis of a larger *Pongo* sample could lead to a better understanding of knee postures/loading of this taxon.

Finally, analyses of sex differences of *Homo* were limited by the lack of sex information for most of the sample. Sex for only 11 (male) individuals was known. These individuals are from Mary Rose population only and thus sex differences could have been tested only by splitting *Homo* populations. However, even though we see partial separation between the populations, the relative PCA positions for rBV/TV and DA remained constant when PCA for studied species was split by *Homo* population (Figure S7).

7 | CONCLUSION

This study provided a holistic approach of trabecular bone architecture within the hominid distal femur. We showed that trabecular pattern distinguishes taxa based on their locomotor repertoires. Trabecular structure in *Homo* reflects habitual use of extended knee postures during bipedalism, habitual use of flexed knee posture during terrestrial and arboreal locomotion in African apes and the highly mobile knee joint in *Pongo*. Moreover, our results reflect differences in the level of knee extension/flexion between female and male *Gorilla*, which is consistent with our current understanding of greater arboreality in female *Gorilla*. Trabecular structure was not significantly different between sexes in *Pan* or *Homo*, which also reflects greater similarity in their locomotor behaviour between sexes. The emergence and form of bipedality in fossil hominins remains a central research focus in paleoanthropology (Barak et al., 2013; Carey & Crompton, 2005; Fajardo et al., 2007; Griffin et al., 2010; Raichlen et al., 2010; Ryan & Ketcham, 2002; Saparin et al., 2011; Shaw & Ryan, 2012; Skinner et al., 2015; Stern Jr & Susman, 1983; Susman, 1991; Susman et al., 1984) and extant great apes are often used to model aspects of fossil hominin locomotor repertoire, including the frequency of arboreality and types of bipedalism (e.g. facultative versus obligate). This study offers a comparative sample of trabecular structure in the hominoid distal femur and can contribute to future studies of locomotion in extinct taxa.

AUTHOR CONTRIBUTIONS

Andrea Lukova conceived and designed the experiments, acquired data, analysed and interpreted the data, prepared figures and tables, authored the first draft and revised subsequent drafts of the article and approved the final manuscript. Christopher J. Dunmore, Sebastian Bachmann, Alexander Synek and Dieter H. Pahr provided tools for data analysis, provided critical revision of the manuscript and approved of the final manuscript. Tracy L. Kivell and Matthew M. Skinner conceived and designed the experiments, contributed data, assisted with the interpretation of the data, provided critical revision of the manuscript and approved the final manuscript.

ACKNOWLEDGEMENTS

For access to specimens in their collections, we thank the following individuals/institutions: Max Planck Institute for Evolutionary Anthropology (C. Boesch, J-J. Hublin); Museum für Naturkunde – Leibniz Institute for Evolution and Biodiversity Science (F. Mayer, C. Funk); Powell-Cotton Museum (I. Livne); Royal Museum for Central Africa (E. Gilissen); University of Florence (J. Moggi-Cecchi, S. Bortoluzzi); Johann-Friedrich-Blumenback-Institute for Zoology and Anthropology, Georg-August University, Goettingen (B. Grosskopf); Frankfurt Senckenberg Museum (V. Volpato); University of the Witswatersand (L. Berger, B. Zipfel); Science Academy of the Czech Republic (J. Svoboda). We thank the Editor-in-Chief, J. Saers and one anonymous reviewer for these constructive comments that greatly improved our manuscript. This project has received funding from the European Research Council (ERC) under the European Union's Horizon 2020 research and innovation programme (grant agreement no. 819960).

DATA AVAILABILITY STATEMENT

Copies of all scans are curated by the relevant curatorial institutions that are responsible for the original specimens and access can be requested through each institution. The authors confirm that the data supporting the findings of this study are available from the corresponding author upon reasonable request.

ORCID

Andrea Lukova https://orcid.org/0009-0001-9843-336X
Christopher J. Dunmore https://orcid.org/0000-0002-8634-9777

REFERENCES

Ahrens, J., Geveci, B., Law, C., Hansen, C. & Johnson, C. (2005) 36-paraview: an end-user tool for large-data visualization. *The Visualization Handbook*, 717, 50038-1.

Alexander, R.M. (1991) Characteristics and advantages of human bipedalism. In: Rayner, J.M.V. & Wooton, R.J. (Eds.) *Biomechanics in evolution*. Cambridge: Cambridge University Press, pp. 225–266.

Alexander, R.M. (2004) Bipedal animals, and their differences from humans. *Journal of Anatomy*, 204(5), 321–330.

Anderson, F.C. & Pandy, M.G. (2001) Dynamic optimization of human walking. *Journal of Biomechanical Engineering*, 123(5), 381–390.

Ankel-Simons, F. (2010) *Primate anatomy: an introduction*. Burlington: Academic press.

Bachmann, S., Dunmore, C.J., Skinner, M.M., Pahr, D.H. & Synek, A. (2022) A computational framework for canonical holistic morphometric analysis of trabecular bone. *Scientific Reports*, 12(1), 5187.

Baltzopoulos, V. (1995) A videofluoroscopy method for optical distortion correction and measurement of knee-joint kinematics. *Clinical Bbiomechanics*, 10(2), 85–92.

Barak, M.M. (2019) Bone modeling or bone remodeling: that is the question. *American Journal of Physical Anthropology*, 172(2), 153–155.

Barak, M.M., Lieberman, D.E. & Hublin, J.J. (2011) A Wolff in sheep's clothing: trabecular bone adaptation in response to changes in joint loading orientation. *Bone*, 49(6), 1141–1151.

Barak, M.M., Lieberman, D.E., Raichlen, D., Pontzer, H., Warrener, A.G. & Hublin, J.J. (2013) Trabecular evidence for a human-like gait in *Australopithecus africanus*. *PLoS One*, 8(11), e77687.

Barak, M.M., Weiner, S. & Shahar, R. (2008) Importance of the integrity of trabecular bone to the relationship between load and deformation of rat femora: an optical metrology study. *Journal of Materials Chemistry*, 18(32), 3855–3864.

Barker, R. (1992) Shipshape for discoveries, and return. *The Mariner's Mirror*, 78(4), 433–447.

Berger, L.R. & Tobias, P.V. (1996) A chimpanzee-like tibia from Sterkfontein, South Africa and its implications for the interpretation of bipedalism in *Australopithecus africanus*. *Journal of Human Evolution*, 30(4), 343–348.

Biewener, A.A., Fazzalari, N.L., Konieczynski, D.D. & Baudinette, R.V. (1996) Adaptive changes in trabecular architecture in relation to functional strain patterns and disuse. *Bone*, 19(1), 1–8.

Cant, J.G. (1987) Positional behavior of female Bornean orangutans (*Pongo pygmaeus*). *American Journal of Primatology*, 12(1), 71–90.

Carey, T.S. & Crompton, R.H. (2005) The metabolic costs of 'bent-hip, bent-knee' walking in humans. *Journal of Human Evolution*, 48(1), 25–44.

Carlson, K.J. (2005) Investigating the form-function interface in African apes: relationships between principal moments of area and positional behaviors in femoral and humeral diaphyses. *American Journal of Physical Anthropology: The Official Publication of the American Association of Physical Anthropologists*, 127(3), 312–334.

Cazenave, M., Braga, J., Oettlé, A., Pickering, T.R., Heaton, J.L., Nakatsukasa, M. et al. (2019) Cortical bone distribution in the femoral neck of *Paranthropus robustus*. *Journal of Human Evolution*, 135, 102666.

Coelho, P.G., Fernandes, P.R., Rodrigues, H.C., Cardoso, J.B. & Guedes, J.M. (2009) Numerical modeling of bone tissue adaptation – a hierarchical approach for bone apparent density and trabecular structure. *Journal of Biomechanics*, 42(7), 830–837.

Cotter, M.M., Simpson, S.W., Latimer, B.M. & Hernandez, C.J. (2009) Trabecular microarchitecture of hominoid thoracic vertebrae. *The Anatomical Record: Advances in Integrative Anatomy and Evolutionary Biology*, 292(8), 1098–1106.

Crompton, R.H., Vereecke, E.E. & Thorpe, S.K. (2008) Locomotion and posture from the common hominoid ancestor to fully modern hominins, with special reference to the last common panin/hominin ancestor. *Journal of Anatomy*, 212(4), 501–543.

Currey, J.D. (2003) The many adaptations of bone. *Journal of Biomechanics*, 36(10), 1487–1495.

Currey, J.D. (2012) The structure and mechanics of bone. *Journal of Materials Science*, 47, 41–54.

Dalstra, M., Huiskes, R., Odgaard, A.V. & Van Erning, L. (1993) Mechanical and textural properties of pelvic trabecular bone. *Journal of Biomechanics*, 26(4–5), 523–535.

D'Août, K., Aerts, P., De Clercq, D., De Meester, K. & Van Elsacker, L. (2002) Segment and joint angles of hind limb during bipedal and quadrupedal walking of the bonobo (*Pan paniscus*). *American Journal of Physical Anthropology: The Official Publication of the American Association of Physical Anthropologists*, 119(1), 37–51.

D'Août, K., Vereecke, E., Schoonaert, K., De Clercq, D., Van Elsacker, L. & Aerts, P. (2004) Locomotion in bonobos (*Pan paniscus*): differences and similarities between bipedal and quadrupedal terrestrial walking, and a comparison with other locomotor modes. *Journal of Anatomy*, 204(5), 353–361.

DeMars, L.J., Kuo, S., Saers, J.P., Stock, J.T. & Ryan, T.M. (2022) Trabecular bone structural variation of the human distal tibia, talus, and calcaneus. *The FASEB Journal*, 36.

Demes, B. (2007) In vivo bone strain and bone functional adaptation. *American Journal of Physical Anthropology*, 133(1), 717–722.

Demes, B., Jungers, W.L. & Walker, C. (2000) Cortical bone distribution in the femoral neck of Strepsirrhine primates. *Journal of Human Evolution*, 39(4), 367–379.

DeSilva, J.M. (2009) Functional morphology of the ankle and the likelihood of climbing in early hominins. *Proceedings of the National Academy of Sciences*, 106(16), 6567–6572.

DeSilva, J.M., Churchill, S.E., Zipfel, B., Walker, C.S., Sylvester, A.D., McNutt, E.J. et al. (2018) *Australopithecus sediba* – the anatomy of the lower limb skeleton of *Australopithecus sediba*. *PaleoAnthropology*, 2018, 357–405.

DeSilva, J.M. & Devlin, M.J. (2012) A comparative study of the trabecular bony architecture of the talus in humans, non-human primates, and *Australopithecus*. *Journal of Human Evolution*, 63(3), 536–551.

Doran, D.M. (1993) Comparative locomotor behavior of chimpanzees and bonobos: The influence of morphology on locomotion. *American Journal of Physical Anthropology*, 91(1), 83–98.

Doran, D.M. (1996) Comparative positional behavior of the African apes. In: McGrew, W., Marchant, L. & Nishida, T. (Eds.) *Great ape societies*. Cambridge: Cambridge University Press, pp. 213–224.

Doran, D.M. (1997) Ontogeny of locomotion in mountain gorillas and chimpanzees. *Journal of Human Evolution*, 32(4), 323–344.

Doube, M., Kłosowski, M.M., Wiktorowicz-Conroy, A.M., Hutchinson, J.R. & Shefelbine, S.J. (2011) Trabecular bone scales allometrically in mammals and birds. *Proceedings of the Royal Society B: Biological Sciences*, 278(1721), 3067–3073.

Dunmore, C.J., Bachmann, S., Synek, A., Pahr, D.H., Skinner, M.M. & Kivell, T.L. (2023) The deep trabecular structure of first metacarpals in extant hominids. *American Journal of Biological* Anthropology.

Dunmore, C.J., Kivell, T.L., Bardo, A. & Skinner, M.M. (2019) Metacarpal trabecular bone varies with distinct hand-positions used in hominid locomotion. *Journal of Anatomy*, 235(1), 45–66.

Dunmore, C.J., Skinner, M.M., Bardo, A., Berger, L.R., Hublin, J.J., Pahr, D.H. et al. (2020) The position of *Australopithecus sediba* within fossil hominin hand use diversity. *Nature Ecology & Evolution*, 4(7), 911–918.

Dunmore, C.J., Wollny, G. & Skinner, M.M. (2018) MIA-clustering: a novel method for segmentation of paleontological material. *PeerJ*, 6, e4374.

Elftman, H. & Manter, J. (1935) The evolution of the human foot, with especial reference to the joints. *Journal of Anatomy*, 70(Pt 1), 56–67.

Eriksen, E.F., Melsen, F. & Mosekilde, L. (1984) Reconstruction of the resorptive site in iliac trabecular bone: A kinetic model for bone resorption in 20 normal individuals. *Metabolic Bone Disease & Related Research*, 5(5), 235–242.

Fajardo, R.J., Müller, R., Ketcham, R.A. & Colbert, M. (2007) Nonhuman anthropoid primate femoral neck trabecular architecture and its relationship to locomotor mode. *The Anatomical Record: Advances in Integrative Anatomy and Evolutionary Biology*, 290(4), 422–436.

Finestone, E.M., Brown, M.H., Ross, S.R. & Pontzer, H. (2018) Great ape walking kinematics: implications for hominoid evolution. *American Journal of Physical Anthropology*, 166(1), 43–55.

Frelat, M.A., Shaw, C.N., Sukhdeo, S., Hublin, J.J., Benazzi, S. & Ryan, T.M. (2017) Evolution of the hominin knee and ankle. *Journal of Human Evolution*, 108, 147–160.

Galdikas, B.M. (1988) Orangutan diet, range, and activity at Tanjung Puting, Central Borneo. *International Journal of Primatology*, 9, 1–35.

Georgiou, L., Dunmore, C.J., Bardo, A., Buck, L.T., Hublin, J.J., Pahr, D.H. et al. (2020) Evidence for habitual climbing in a Pleistocene hominin in South Africa. *Proceedings of the National Academy of Sciences*, 117(15), 8416–8423.

Georgiou, L., Kivell, T.L., Pahr, D.H., Buck, L.T. & Skinner, M.M. (2019) Trabecular architecture of the great ape and human femoral head. *Journal of Anatomy*, 234(5), 679–693.

Georgiou, L., Kivell, T.L., Pahr, D.H. & Skinner, M.M. (2018) Trabecular bone patterning in the hominoid distal femur. *PeerJ*, 6, e5156.

Girgis, F.G., Marshall, J.L. & Jem, A.A.M. (1975) The cruciate ligaments of the knee joint: anatomical. Functional and experimental analysis. *Clinical Orthopaedics and Related Research®*, 106, 216–231.

Glatt, V., Canalis, E., Stadmeyer, L. & Bouxsein, M.L. (2007) Age-related changes in trabecular architecture differ in female and male C57BL/6J mice. *Journal of Bone and Mineral Research*, 22(8), 1197–1207.

Goh, C., Blanchard, M.L., Crompton, R.H., Gunther, M.M., Macaulay, S. & Bates, K.T. (2017) A 3D musculoskeletal model of the western lowland gorilla hind limb: moment arms and torque of the hip, knee and ankle. *Journal of Anatomy*, 231(4), 568–584.

Griffin, N.L., D'Août, K., Ryan, T.M., Richmond, B.G., Ketcham, R.A. & Postnov, A. (2010) Comparative forefoot trabecular bone architecture in extant hominids. *Journal of Human Evolution*, 59(2), 202–213.

Gross, T., Kivell, T.L., Skinner, M.M., Nguyen, N.H. & Pahr, D.H. (2014) A CT-image-based method for the holistic analysis of cortical and trabecular bone. *Submitted to Pal Elec*, 17, 33A.

Haile-Selassie, Y., Saylor, B.Z., Deino, A., Levin, N.E., Alene, M. & Latimer, B.M. (2012) A new hominin foot from Ethiopia shows multiple Pliocene bipedal adaptations. *Nature*, 483(7391), 565–569.

Halloran, B.P., Ferguson, V.L., Simske, S.J., Burghardt, A., Venton, L.L. & Majumdar, S. (2002) Changes in bone structure and mass with advancing age in the male C57BL/6J mouse. *Journal of Bone and Mineral Research*, 17(6), 1044–1050.

Hammond, A.S. (2014) In vivo baseline measurements of hip joint range of motion in suspensory and nonsuspensory anthropoids. *American Journal of Physical Anthropology*, 153(3), 417–434.

Harcourt-Smith, W. (2016) Early hominin diversity and the emergence of the genus *Homo*. *Journal of Anthropological Sciences*, 94, 19–27.

Harcourt-Smith, W.E., Throckmorton, Z., Congdon, K.A., Zipfel, B., Deane, A.S., Drapeau, M.S. et al. (2015) The foot of *Homo naledi*. *Nature Communications*, 6(1), 8432.

Hardt, D.E. (1978) Determining muscle forces in the leg during normal human walking – an application and evaluation of optimization methods. *Journal of Biomechanical Engineering*, 100(2), 72–78.

Harrison, L.C., Nikander, R., Sikiö, M., Luukkaala, T., Helminen, M.T., Ryymin, P. et al. (2011) MRI texture analysis of femoral neck: detection of exercise load-associated differences in trabecular bone. *Journal of Magnetic Resonance Imaging*, 34(6), 1359–1366.

Hirschmann, M.T. & Müller, W. (2015) Complex function of the knee joint: the current understanding of the knee. *Knee Surgery, Sports Traumatology, Arthroscopy*, 23, 2780–2788.

Homminga, J., Mccreadie, B.R., Weinans, H. & Huiskes, R. (2003) The dependence of the elastic properties of osteoporotic cancellous bone on volume fraction and fabric. *Journal of Biomechanics*, 36(10), 1461–1467.

Huijing, P.A. (1985) Architecture of the human gastrocnemius muscle and some functional consequences. *Cells, Tissues, Organs*, 123(2), 101–107.

Ishikawa, M., Pakaslahti, J. & Komi, P.V. (2007) Medial gastrocnemius muscle behavior during human running and walking. *Gait & Posture*, 25(3), 380–384.

Isler, K. (2005) 3D-kinematics of vertical climbing in hominoids. *American Journal of Physical Anthropology: The Official Publication of the American Association of Physical Anthropologists*, 126(1), 66–81.

Javois, C., Tardieu, C., Lebel, B., Seil, R., Hulet, C. & Société française d'arthroscopie. (2009) Comparative anatomy of the knee joint: effects on the lateral meniscus. *Orthopaedics & Traumatology, Surgery & Research*, 95(8), 49–59.

Kamibayashi, L., Wyss, U.P., Cooke, T.D.V. & Zee, B. (1995) Trabecular microstructure in the medial condyle of the proximal tibia of patients with knee osteoarthritis. *Bone*, 17(1), 27–35.

Kozma, E.E., Webb, N.M., Harcourt-Smith, W.E., Raichlen, D.A., D'Août, K., Brown, M.H. et al. (2018) Hip extensor mechanics and the evolution of walking and climbing capabilities in humans, apes, and fossil hominins. *Proceedings of the National Academy of Sciences*, 115(16), 4134–4139.

Krevolin, J.L., Pandy, M.G. & Pearce, J.C. (2004) Moment arm of the patellar tendon in the human knee. *Journal of Biomechanics*, 37(5), 785–788.

Kuo, S., Saers, J.P., Scott, R.S. & Ryan, T.M. (2022) Trabecular and cortical bone morphology of the distal radius in humans, chimpanzees, cercopithecids, and anteaters. *The FASEB Journal*, 36.

Landis, E.K. & Karnick, P. (2006) A three-dimensional analysis of the geometry and curvature of the proximal tibial articular surface of hominoids. *In Three-Dimensional Image Capture and Applications VII*, 6056, 189–200.

Lee, L.F., O'Neill, M.C., Demes, B., LaBoda, M.D., Thompson, N.E., Larson, S.G. et al. (2012) Joint kinematics in chimpanzee and human bipedal walking. *The Hip*, 20(10), 32–42.

Lichtwark, G.A., Bougoulias, K. & Wilson, A.M. (2007) Muscle fascicle and series elastic element length changes along the length of the human gastrocnemius during walking and running. *Journal of Biomechanics*, 40(1), 157–164.

Loewen, N., Fautsch, M.P., Peretz, M., Bahler, C.K., Cameron, J.D., Johnson, D.H. et al. (2001) Genetic modification of human trabecular meshwork with lentiviral vectors. *Human Gene Therapy*, 12(17), 2109–2119.

Loudon, J.K. (2016) Biomechanics and pathomechanics of the patellofemoral joint. *International Journal of Sports Physical Therapy*, 11(6), 820–830.

Lovejoy, C.O. (1988) Evolution of human walking. *Scientific American*, 259(5), 118–125.

Lovejoy, C.O. (2007) The natural history of human gait and posture: part 3. *The Knee Gait & Posture*, 25(3), 325–341.

Lovejoy, C.O., Simpson, S.W., White, T.D., Asfaw, B. & Suwa, G. (2009) Careful climbing in the Miocene: the forelimbs of *Ardipithecus ramidus* and humans are primitive. *Sciences*, 326(5949), 70-70e8.

Maganaris, C.N. (2003) Force-length characteristics of the in vivo human gastrocnemius muscle. *Clinical Anatomy: The Official Journal of the American Association of Clinical Anatomists and the British Association of Clinical Anatomists*, 16(3), 215–223.

Mann, R.A. & Hagy, J. (1980) Biomechanics of walking, running, and sprinting. *The American Journal of Sports Medicine*, 8(5), 345–350.

Maquer, G., Musy, S.N., Wandel, J., Gross, T. & Zysset, P.K. (2015) Bone volume fraction and fabric anisotropy are better determinants of trabecular bone stiffness than other morphological variables. *Journal of Bone and Mineral Research*, 30(6), 1000–1008.

Masouros, S.D., Bull, A.M.J. & Amis, A.A. (2010) Biomechanics of the knee joint. *Orthopaedics and Traumatology*, 24(2), 84–91.

Mazurier, A., Nakatsukasa, M. & Macchiarelli, R. (2010) The inner structural variation of the primate tibial plateau characterized by high-resolution microtomography. Implications for the reconstruction of fossil locomotor behaviours. *Comptes Rendus Palevol*, 9(6–7), 349–359.

Mittra, E., Rubin, C. & Qin, Y.X. (2005) Interrelationship of trabecular mechanical and microstructural properties in sheep trabecular bone. *Journal of Biomechanics*, 38(6), 1229–1237.

Morbeck, M.E. & Zihlman, A.L. (1989) Body size and proportions in chimpanzees, with special reference to *Pan troglodytes schweinfurthii* from Gombe National Park, Tanzania. *Primates*, 30, 369–382.

Muramatsu, T., Muraoka, T., Takeshita, D., Kawakami, Y., Hirano, Y. & Fukunaga, T. (2001) Mechanical properties of tendon and aponeurosis of human gastrocnemius muscle in vivo. *Journal of Applied Physiology*, 90(5), 1671–1678.

Napier, J. (1967) The antiquity of human walking. *Scientific American*, 216(4), 56–67.

Neptune, R.R. & Kautz, S.A. (2001) Muscle activation and deactivation dynamics: the governing properties in fast cyclical human movement performance? *Exercise and Sport Sciences Reviews*, 29(2), 76–81.

Nilsson, J. & Thorstensson, A. (1987) Adaptability in frequency and amplitude of leg movements during human locomotion at different speeds. *Acta Physiologica Scandinavica*, 129(1), 107–114.

Nordin, M. & Frankel, V.H. (Eds.). (2001) *Basic biomechanics of the musculoskeletal system*. 3rd ed. Philadelphia, PA: Lippincott Williams & Wilkins.

Novitskaya, E., Zin, C., Chang, N., Cory, E., Chen, P., D'Lima, D. et al. (2014) Creep of trabecular bone from the human proximal tibia. *Materials Science and Engineering: C*, 40, 219–227.

Odgaard, A., Kabel, J., van Rietbergen, B., Dalstra, M. & Huiskes, R. (1997) Fabric and elastic principal directions of cancellous bone are closely related. *Journal of Biomechanics*, 30(5), 487–495.

Ohman, J.C., Krochta, T.J., Lovejoy, C.O., Mensforth, R.P. & Latimer, B. (1997) Cortical bone distribution in the femoral neck of hominoids: implications for the locomotion of *Australopithecus afarensis*. *American Journal of Physical Anthropology: The Official Publication of the American Association of Physical Anthropologists*, 104(1), 117–131.

Organ, J.M. & Ward, C.V. (2006) Contours of the hominoid lateral tibial condyle with implications for *Australopithecus*. *Journal of Human Evolution*, 51(2), 113–127.

Pahr, D.H. & Zysset, P.K. (2009) From high-resolution CT data to finite element models: development of an integrated modular framework. *Computer Methods in Biomechanics and Biomedical Engineering*, 12(1), 45–57.

Paternoster, L., Lorentzon, M., Lehtimäki, T., Eriksson, J., Kähönen, M., Raitakari, O. et al. (2013) Genetic determinants of trabecular and cortical volumetric bone mineral densities and bone microstructure. *PLoS Genetics*, 9(2), e1003247.

Payne, R.C., Crompton, R.H., Isler, K., Savage, R., Vereecke, E.E., Günther, M.M. et al. (2006) Morphological analysis of the hindlimb in apes and humans. I. Muscle architecture. *Journal of Anatomy*, 208(6), 709–724.

Pearson, O.M. & Lieberman, D.E. (2004) The aging of Wolff's "law": ontogeny and responses to mechanical loading in cortical bone. *American Journal of Physical Anthropology*, 125(S39), 63–99.

Pina, M., Almecija, S., Alba, D.M., O'Neill, M.C. & Moya-Sola, S. (2014) The middle Miocene ape *Pierolapithecus catalaunicus* exhibits extant great ape-like morphometric affinities on its patella: inferences on knee function and evolution. *PLoS One*, 9(3), e91944.

Pontzer, H., Lieberman, D.E., Momin, E., Devlin, M.J., Polk, J.D., Hallgrimsson, B. et al. (2006) Trabecular bone in the bird knee responds with high sensitivity to changes in load orientation. *Journal of Experimental Biology*, 209(1), 57–65.

Pontzer, H., Raichlen, D.A. & Sockol, M.D. (2009) The metabolic cost of walking in humans, chimpanzees, and early hominins. *Journal of Human Evolution*, 56(1), 43–54.

Preuschof, H. & Tardieu, C. (1996) Biomechanical reasons for the divergent morphology of the knee joint and the distal epiphyseal suture in hominoids. *Folia Primatologica*, 66(1–4), 82–92.

Racic, V., Pavic, A. & Brownjohn, J.M.W. (2009) Experimental identification and analytical modelling of human walking forces: literature review. *Journal of Sound and Vibration*, 326(1–2), 1–49.

Rafferty, K.L. (1998) Erratum structural design of the femoral neck in primates. *Journal of Human Evolution*, 35, 109–383.

Raichlen, D.A., Gordon, A.D., Harcourt-Smith, W.E., Foster, A.D. & Haas, W.R., Jr. (2010) Laetoli footprints preserve earliest direct evidence of human-like bipedal biomechanics. *PLoS One*, 5(3), e9769.

Remis, M. (1995) Effects of body size and social context on the arboreal activities of lowland gorillas in the Central African Republic. *American Journal of Physical Anthropology*, 97(4), 413–433.

Remis, M.J. (1994) *Feeding ecology and positional behavior of western lowland gorillas (Gorilla gorilla gorilla) in the Central African Republic*. Ph.D. dissertation. Yale University Press London.

Rodan, G.A. (1997) Bone mass homeostasis and bisphosphonate action. *Bone*, 20(1), 1–4.

Rubin, C., Turner, A.S., Mallinckrodt, C., Jerome, C., McLeod, K. & Bain, S. (2002) Mechanical strain, induced noninvasively in the high-frequency domain, is anabolic to cancellous bone, but not cortical bone. *Bone*, 30(3), 445–452.

Rueckert, D., Frangi, A.F. & Schnabel, J.A. (2003) Automatic construction of 3-D statistical deformation models of the brain using nonrigid registration. *IEEE Transactions on Medical Imaging*, 22(8), 1014–1025.

Ruff, C., Holt, B. & Trinkaus, E. (2006) Who's afraid of the big bad Wolff?:"Wolff's law" and bone functional adaptation. *American Journal of Physical Anthropology: The Official Publication of the American Association of Physical Anthropologists*, 129(4), 484–498.

Ruff, C.B. (2002) Long bone articular and diaphyseal structure in Old World monkeys and apes. I: locomotor effects. *American Journal of Physical Anthropology: The Official Publication of the American Association of Physical Anthropologists*, 119(4), 305–342.

Ruff, C.B., Burgess, M.L., Bromage, T.G., Mudakikwa, A. & McFarlin, S.C. (2013) Ontogenetic changes in limb bone structural proportions in mountain gorillas (*Gorilla beringei beringei*). *Journal of Human Evolution*, 65(6), 693–703.

Ryan, T.M. & Ketcham, R.A. (2002) The three-dimensional structure of trabecular bone in the femoral head of Strepsirrhine primates. *Journal of Human Evolution*, 43(1), 1–26.

Ryan, T.M. & Shaw, C.N. (2013) Trabecular bone microstructure scales allometrically in the primate humerus and femur. *Proceedings of the Royal Society B: Biological Sciences*, 280(1758), 20130172.

Ryan, T.M., Stephens, N., Doershuk, L.J., Saers, J.P., Jashashvili, T., Carlson, K.J. et al. (2019) Trabecular bone structural variation in the human postcranial skeleton. *The FASEB Journal*, 33(S1), 19.2.

Ryan, T.M. & Walker, A. (2010) Trabecular bone structure in the humeral and femoral heads of anthropoid primates. *The Anatomical Record: Advances in Integrative Anatomy and Evolutionary Biology*, 293(4), 719–729.

Saers, J.P., Cazorla-Bak, Y., Shaw, C.N., Stock, J.T. & Ryan, T.M. (2016) Trabecular bone structural variation throughout the human lower limb. *Journal of Human Evolution*, 97, 97–108.

Saers, J.P., Gordon, A.D., Ryan, T.M. & Stock, J.T. (2022) Trabecular bone ontogeny tracks neural development and life history among humans and non-human primates. *Proceedings of the National Academy of Sciences*, 119(49), e2208772119.

Saers, J.P., Ryan, T.M. & Stock, J.T. (2019) Trabecular bone functional adaptation and sexual dimorphism in the human foot. *American Journal of Physical Anthropology*, 168(1), 154–169.

Saers, J.P., Ryan, T.M. & Stock, J.T. (2020) Baby steps towards linking calcaneal trabecular bone ontogeny and the development of bipedal human gait. *Journal of Anatomy*, 236(3), 474–492.

Saparin, P., Scherf, H., Hublin, J.J., Fratzl, P. & Weinkamer, R. (2011) Structural adaptation of trabecular bone revealed by position resolved analysis of proximal femora of different primates. *The Anatomical Record: Advances in Integrative Anatomy and Evolutionary Biology*, 294(1), 55–67.

Scorrer, J., Faillace, K.E., Hildred, A., Nederbragt, A.J., Andersen, M.B., Millet, M.A. et al. (2021) Diversity aboard a Tudor warship: investigating the origins of the Mary Rose crew using multi-isotope analysis. *Royal Society Open Science*, 8(5), 202106.

Seeman, E. (2003) Invited review: pathogenesis of osteoporosis. *Journal of Applied Physiology*, 95(5), 2142–2151.

Shaw, C.N. & Ryan, T.M. (2012) Does skeletal anatomy reflect adaptation to locomotor patterns? Cortical and trabecular architecture in human and nonhuman anthropoids. *American Journal of Physical Anthropology*, 147(2), 187–200.

Simpson, K.J. & Pettit, M.I.C.H.A.E.L. (1997) Jump distance of dance landings influencing internal joint forces: II. Shear forces. *Medicine and Science in Sports and Exercise*, 29(7), 928–936.

Sinclair, K.D., Farnsworth, R.W., Pham, T.X., Knight, A.N., Bloebaum, R.D. & Skedros, J.G. (2013) The artiodactyl calcaneus as a potential 'control bone' cautions against simple interpretations of trabecular bone adaptation in the anthropoid femoral neck. *Journal of Human Evolution*, 64(5), 366–379.

Skinner, M., Tsegai, Z.J., Kivell, T.L., Gross, T., Nguyen, N.H., Pahr, D.H. et al. (2013) Trabecular bone structure correlates with hand posture and use in hominoids. *PLoS One*, 8(11), 1–14.

Skinner, M.M., Stephens, N.B., Tsegai, Z.J., Foote, A.C., Nguyen, N.H., Gross, T. et al. (2015) Human-like hand use in *Australopithecus africanus*. *Science*, 347(6220), 395–399.

Smith, R.J. & Jungers, W.L. (1997) Body mass in comparative primatology. *Journal of Human Evolution*, 32(6), 523–559.

Spoor, C.W. & Van Leeuwen, J.L. (1992) Knee muscle moment arms from MRI and from tendon travel. *Journal of Biomechanics*, 25(2), 201–206.

Steiner, L., Synek, A. & Pahr, D.H. (2021) Femoral strength can be predicted from 2D projections using a 3D statistical deformation and texture model with finite element analysis. *Medical Engineering & Physics*, 93, 72–82.

Stephens, N.B., Kivell, T.L., Gross, T., Pahr, D.H., Lazenby, R.A., Hublin, J.J. et al. (2016) Trabecular architecture in the thumb of *Pan* and *Homo*: implications for investigating hand use, loading, and hand preference in the fossil record. *American Journal of Physical Anthropology*, 161(4), 603–619.

Stern, J.T., Jr. & Susman, R.L. (1981) Electromyography of the gluteal muscles in *Hylobates*, *Pongo*, and *Pan*: implications for the evolution of hominid bipedality. *American Journal of Physical Anthropology*, 55(2), 153–166.

Stern, J.T., Jr. & Susman, R.L. (1983) The locomotor anatomy of *Australopithecus afarensis*. *American Journal of Physical Anthropology*, 60(3), 279–317.

Stirland, A.J. & Waldron, T. (1997) Evidence for activity related markers in the vertebrae of the crew of the Mary Rose. *Journal of Archaeological Science*, 24(4), 329–335.

Su, A., Wallace, I.J. & Nakatsukasa, M. (2013) Trabecular bone anisotropy and orientation in an Early Pleistocene hominin talus from East Turkana, Kenya. *Journal of Human Evolution*, 64(6), 667–677.

Sugiyama, T., Neuhaus, M., Cole, R., Giles-Corti, B. & Owen, N. (2012) Destination and route attributes associated with adults' walking: a review. *Medicine and Science in Sports and Exercise*, 44(7), 1275–1286.

Sukhdeo, S., Parsons, J., Niu, X.M. & Ryan, T.M. (2020) Trabecular bone structure in the distal femur of humans, apes, and baboons. *The Anatomical Record*, 303(1), 129–149.

Susman, R.L. (1991) Who made the Oldowan tools? Fossil evidence for tool behavior in Plio-Pleistocene hominids. *Journal of Anthropological Research*, 47(2), 129–151.

Susman, R.L., Stern, J.T. & Jungers, W.L. (1984) Arboreality and bipedality in the Hadar hominids. *Folia Primatologica*, 43(2–3), 113–156.

Sylvester, A.D. (2013) A geometric morphometric analysis of the medial tibial condyle of African hominids. *The Anatomical Record*, 296(10), 1518–1525.

Sylvester, A.D., Mahfouz, M.R. & Kramer, P.A. (2011) The effective mechanical advantage of AL 129-1a for knee extension. *The Anatomical Record: Advances in Integrative Anatomy and Evolutionary Biology*, 294(9), 1486–1499.

Sylvester, A.D. & Organ, J.M. (2010) Curvature scaling in the medial tibial condyle of large bodied hominoids. *The Anatomical Record: Advances in Integrative Anatomy and Evolutionary Biology*, 293(4), 671–679.

Sylvester, A.D. & Pfisterer, T. (2012) Quantifying lateral femoral condyle ellipticalness in chimpanzees, gorillas, and humans. *American Journal of Physical Anthropology*, 149(3), 458–467.

Sylvester, A.D. & Terhune, C.E. (2017) Trabecular mapping: leveraging geometric morphometrics for analyses of trabecular structure. *American Journal of Physical Anthropology*, 163(3), 553–569.

Tardieu, C. (1999) Ontogeny and phylogeny of femoro-tibial characters in humans and hominid fossils: functional influence and genetic determinism. *American Journal of Physical Anthropology: The Official Publication of the American Association of Physical Anthropologists*, 110(3), 365–377.

Taylor, W.R., Heller, M.O., Bergmann, G. & Duda, G.N. (2004) Tibiofemoral loading during human gait and stair climbing. *Journal of Orthopaedic Research*, 22(3), 625–632.

Thompson, N.E., Ostrofsky, K.R., McFarlin, S.C., Robbins, M.M., Stoinski, T.S. & Almecija, S. (2018) Unexpected terrestrial hand posture

diversity in wild mountain gorillas. *American Journal of Physical Anthropology*, 166(1), 84–94.

Thomsen, J.S., Laib, A., Koller, B., Prohaska, S., Mosekilde, L.I. & Gowin, W. (2005) Stereological measures of trabecular bone structure: comparison of 3D micro computed tomography with 2D histological sections in human proximal tibial bone biopsies. *Journal of Microscopy*, 218(2), 171–179.

Thorpe, S.K. & Crompton, R.H. (2005) Locomotor ecology of wild orangutans (*Pongo pygmaeus abelii*) in the Gunung Leuser Ecosystem, Sumatra, Indonesia: a multivariate analysis using log-linear modelling. *American Journal of Physical Anthropology: The Official Publication of the American Association of Physical Anthropologists*, 127(1), 58–78.

Thorpe, S.K. & Crompton, R.H. (2006) Orangutan positional behavior and the nature of arboreal locomotion in Hominoidea. *American Journal of Physical Anthropology: The Official Publication of the American Association of Physical Anthropologists*, 131(3), 384–401.

Thorpe, S.K., Holder, R. & Crompton, R.H. (2009) Orangutans employ unique strategies to control branch flexibility. *Proceedings of the National Academy of Sciences*, 106(31), 12646–12651.

Thorpe, S.K., Holder, R.L. & Crompton, R.H. (2007) Origin of human bipedalism as an adaptation for locomotion on flexible branches. *Science*, 316(5829), 1328–1331.

Tocheri, M.W., Solhan, C.R., Orr, C.M., Femiani, J., Frohlich, B., Groves, C.P. et al. (2011) Ecological divergence and medial cuneiform morphology in gorillas. *Journal of Human Evolution*, 60(2), 171–184.

Tsegai, Z.J., Skinner, M.M., Gee, A.H., Pahr, D.H., Treece, G.M., Hublin, J.J. et al. (2017) Trabecular and cortical bone structure of the talus and distal tibia in *Pan* and *Homo*. *American Journal of Physical Anthropology*, 163(4), 784–805.

Tsegai, Z.J., Skinner, M.M., Pahr, D.H., Hublin, J.J. & Kivell, T.L. (2018) Ontogeny and variability of trabecular bone in the chimpanzee humerus, femur and tibia. *American Journal of Physical Anthropology*, 167(4), 713–736.

Tsegai, Z.J., Stephens, N.B., Treece, G.M., Skinner, M.M., Kivell, T.L. & Gee, A.H. (2017) Cortical bone mapping: an application to hand and foot bones in hominoids. *Comptes Rendus Palevol*, 16(5–6), 690–701.

Turner, C.H., Hsieh, Y.F., Müller, R., Bouxsein, M.L., Baylink, D.J., Rosen, C.J. et al. (2000) Genetic regulation of cortical and trabecular bone strength and microstructure in inbred strains of mice. *Journal of Bone and Mineral Research*, 15(6), 1126–1131.

Van Rietbergen, B., Odgaard, A., Kabel, J. & Huiskes, R. (1998) Relationships between bone morphology and bone elastic properties can be accurately quantified using high-resolution computer reconstructions. *Journal of Orthopaedic Research*, 16(1), 23–28.

Visser, J.J., Hoogkamer, J.E., Bobbert, M.F. & Huijing, P.A. (1990) Length and moment arm of human leg muscles as a function of knee and hip-joint angles. *European Journal of Applied Physiology and Occupational Physiology*, 61, 453–460.

Volpato, V., Viola, T.B., Nakatsukasa, M., Bondioli, L. & Macchiarelli, R. (2008) Textural characteristics of the iliac-femoral trabecular pattern in a bipedally trained Japanese macaque. *Primates*, 49, 16–25.

Wallace, I.J., Kwaczala, A.T., Judex, S., Demes, B. & Carlson, K.J. (2013) Physical activity engendering loads from diverse directions augments the growing skeleton. *Journal of Musculoskeletal & Neuronal Interactions*, 13(3), 283–288.

Wanner, J.A. (1977) Variations in the anterior patellar groove of the human femur. *American Journal of Physical Anthropology*, 47(1), 99–102.

Whitehouse, W.J. (1977) Cancellous bone in the anterior part of the iliac crest. *Calcified Tissue Research*, 23, 67–76.

Zaharie, D.T. & Phillips, A.T. (2018) Pelvic construct prediction of trabecular and cortical bone structural architecture. *Journal of Biomechanical Engineering*, 140(9), 091001.

Zheng, N., Fleisig, G.S., Escamilla, R.F. & Barrentine, S.W. (1998) An analytical model of the knee for estimation of internal forces during exercise. *Journal of Biomechanics*, 31(10), 963–967.

Zihlman, A.L., Mcfarland, R.K. & Underwood, C.E. (2011) Functional anatomy and adaptation of male gorillas (*Gorilla gorilla gorilla*) with comparison to male orangutans (*Pongo pygmaeus*). *The Anatomical Record: Advances in Integrative Anatomy and Evolutionary Biology*, 294(11), 1842–1855.

Zysset, P.K. (2003) A review of morphology–elasticity relationships in human trabecular bone: theories and experiments. *Journal of Biomechanics*, 36(10), 1469–1485.

SUPPORTING INFORMATION

Additional supporting information can be found online in the Supporting Information section at the end of this article.

How to cite this article: Lukova, A., Dunmore, C.J., Bachmann, S., Synek, A., Pahr, D.H., Kivell, T.L. et al. (2024) Trabecular architecture of the distal femur in extant hominids. *Journal of Anatomy*, 00, 1–25. Available from: https://doi.org/10.1111/joa.14026